Compositional Mapping

J. Goldstein et al., *Scanning Electron Microscopy and X-Ray Microanalysis*,
https://doi.org/10.1007/978-1-4939-6676-9_24

SEM images that show the spatial distribution of the elemental constituents of a specimen ("elemental maps") can be created by using the characteristic X-ray intensity measured for each element with the energy dispersive X-ray spectrometer (EDS) to define the gray level (or color value) at each picture element (pixel) of the scan. Elemental maps based on X-ray intensity provide qualitative information on spatial distributions of elements. Compositional mapping, in which a full EDS spectrum is recorded at each pixel ("X-ray Spectrum Imaging" or XSI) and processed with peak fitting, k-ratio standardization, and matrix corrections, provides a quantitative basis for comparing maps of different elements in the same region, or for the same element from different regions.

24.1 Total Intensity Region-of-Interest Mapping

In the simplest implementation of elemental mapping, energy regions are defined in the spectrum that span the characteristic X-ray peak(s) of interest, as shown in Fig. 24.1. The total X-ray intensity (counts) within each energy region, I_{Xi}, consisting of both the characteristic peak intensity, including any overlapping peaks, and the continuum background intensity, is digitally recorded for each pixel, creating a set of x-y-I_{Xi} image arrays for the defined suite of elements. Depending on the local concentration of an element, the overvoltage $U_0 = E_0/E_c$ for the measured characteristic peak, the beam current, the solid angle of the detector, and the dwell time per pixel, the number of counts per elemental window can vary widely from a few counts per pixel to several thousand or more. A typical strategy to avoid saturation is to collect 2-byte deep X-ray intensity data that permits up to 65,536 counts per energy region per pixel. In common with the practice for BSE and SE images, the final elemental map will be displayed with a 1-byte intensity range (0–255 gray levels). To maximize the contrast within each map it is necessary to nearly fill this display range so that it is common practice to automatically scale ("autoscale") the measured intensity in a linear fashion to span slightly less than 1-byte. The displayed gray levels are scaled to range from near black, but avoiding black (gray level zero) to avoid clipping, to near white, but avoiding full white (gray level 255), to prevent saturation. The counts are expanded for elements that span less than 1-byte in the original data collection, while the counts are compressed for elements that extend into the 2-byte range. An example of such total intensity mapping is shown in Fig. 24.2, which presents a set of maps for Si, Fe, and Mn in a cross section of a deep-sea manganese nodule with a complex microstructure. The EDS spectrum shown in Fig. 24.1 also reveals a typical problem encountered in simple intensity window mapping. Manganese is one of the most abundant elements in this specimen, and the Mn K-$M_{2,3}$ (6.490 keV) interferes with Fe K-$L_{2,3}$ (6.400 keV), which is especially significant since iron is a minor/trace constituent. To avoid the potential artifacts in this situation, the analyst can instead choose the Fe K-$M_{2,3}$ (7.057 keV) which does not suffer the interference but which is approximately a factor of ten lower intensity than Fe K-$L_{2,3}$. While sacrificing sensitivity, the

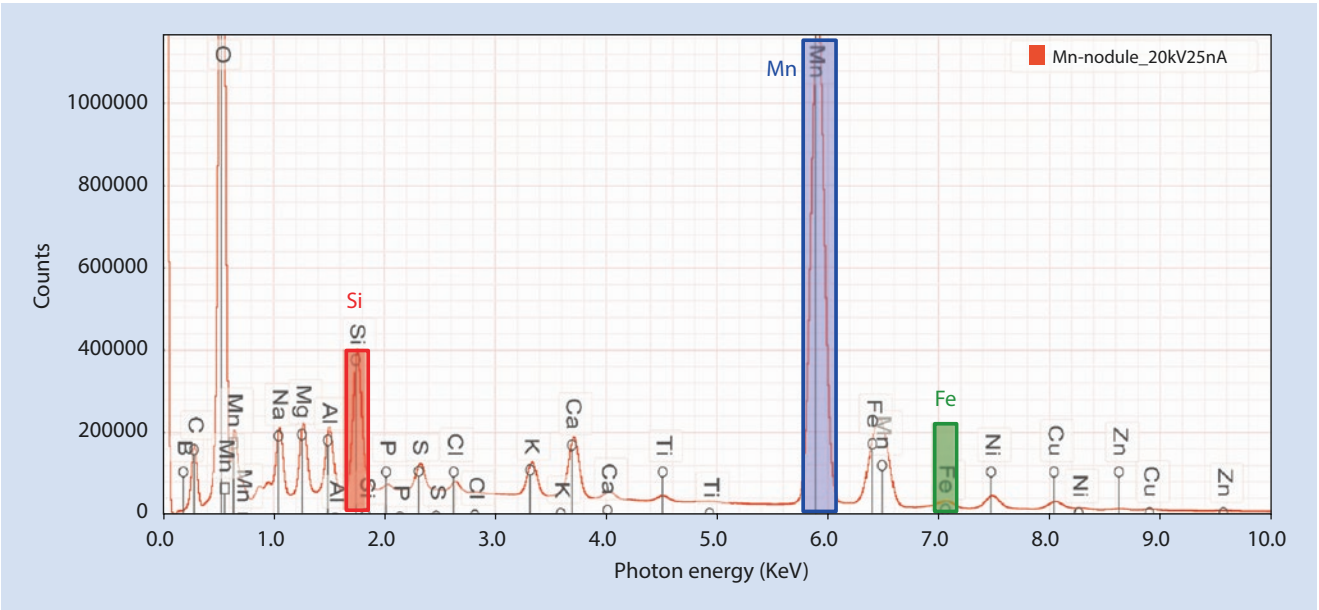

Fig. 24.1 EDS spectrum measured on a cross section of a deep-sea manganese nodule showing peak selection (Si K-L_2, Mn K-$L_{2,3}$, and Fe K-$M_{2,3}$) for total intensity elemental mapping

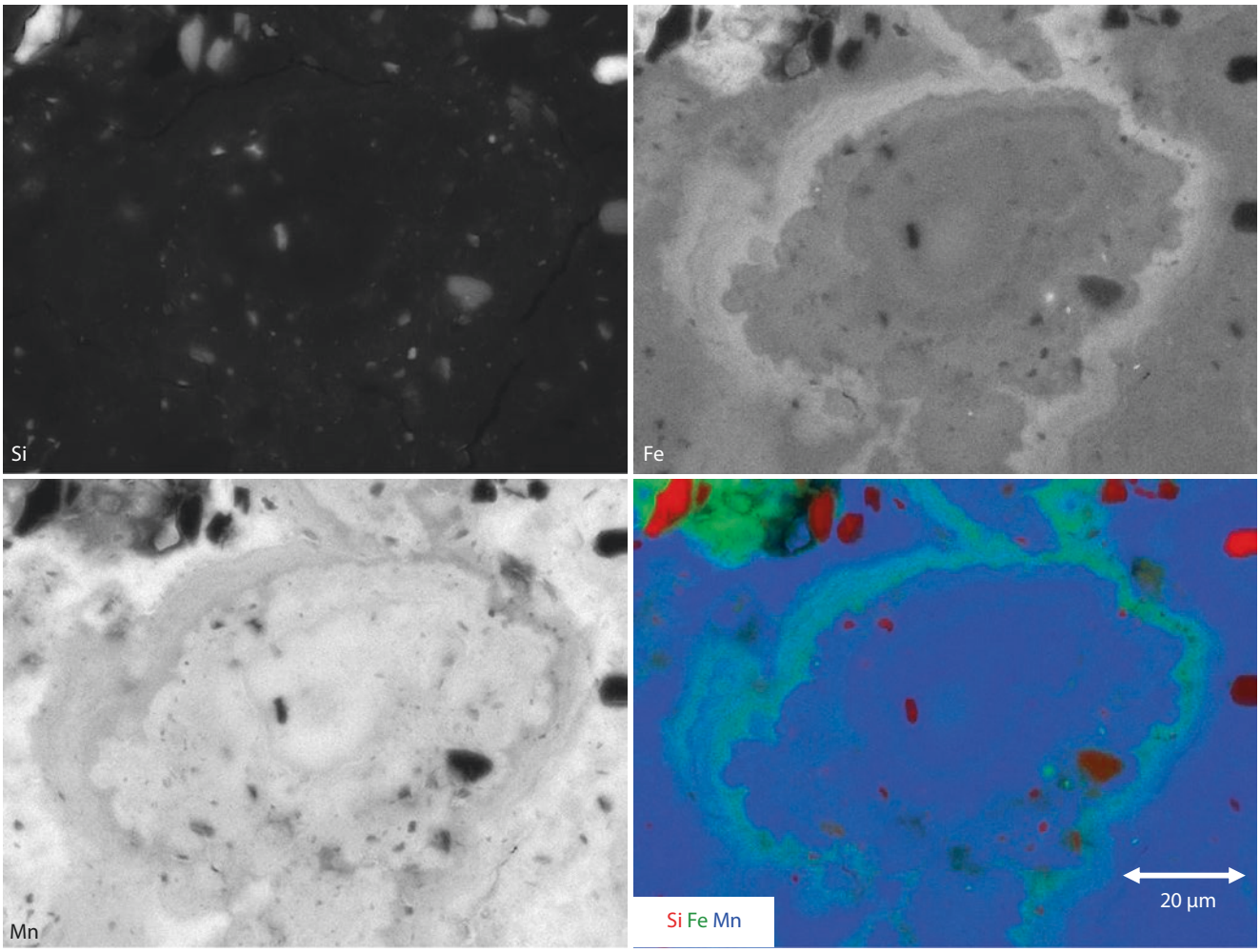

Fig. 24.2 Total intensity elemental maps for Si K-L_2, Mn K-$L_{2,3}$, and Fe K-$M_{2,3}$ measured on a cross section of a deep-sea manganese nodule, and the color overlay of the gray-scale maps

success of this strategy is revealed in Fig. 24.2, where the major Mn and minor Fe are seen to be anti-correlated.

Figure 24.2 also contains a primary color overlay of these three elements, encoded with Si in red, Fe in green, and Mn in blue, a commonly used image display tool which provides an immediate visual comparison of the relative spatial relationships of the three constituents. The appearance of secondary colors shows areas of coincidence of any two elements, for example, the cyan colored region is a combination of green and blue and thus shows the coincidence of Fe and Mn. The other possible binary combinations are yellow (red plus green, Si + Fe) and magenta (red plus blue, Si + Mn), which are not present in this example. If all three elements were present at the same location, white would result.

24.1.1 Limitations of Total Intensity Mapping

While total intensity elemental maps such as those in Fig. 24.2 are useful for developing a basic understanding of the spatial distributions of the elements that make up the specimen, total intensity mapping is subject to several significant limitations:

1. By selecting only the spectral regions-of-interest, the amount of mass storage is minimized. However, while all spectral regions-of-interest are collected simultaneously, if the analyst needs to evaluate another element not originally selected when the data was collected, the entire image scan must be repeated to recollect the data with that new element included.

2. Total intensity maps convey qualitative information only. The elemental spatial distributions are meaningful only in qualitative terms of interpreting which elements are present at a particular pixel location(s) by comparing different elemental maps of the same area, for example, using the color overlay method. Since the images are recorded simultaneously, the pixel registration is without error even if overall drift or other distortion occurs. However, the intensity information is not quantitative and can only convey relative abundance information within an individual elemental map (e.g., "this location has more of element A than this location because the intensity of A is higher"). The gray levels in maps for different elements cannot be readily compared because the X-ray intensity for each element that defines the gray level range of the map is determined by the local concentration and the complex physics of X-ray generation, propagation, and detection efficiency, all of which vary with the elemental species. The element-to-element differences in the efficiency of X-ray production, propagation, and detection are embedded in the raw measured X-ray intensities, which are then subjected to the autoscaling operation. Unless the autoscaling factor is recorded (typically not), it is not possible after the fact to recover the information that would enable the analyst to standardize and establish a proper basis for inter-comparison of maps of different elements, or even of maps of the same element from different areas. Thus, the sequence of gray levels only has interpretable meaning within an individual elemental map. Gray levels cannot be sensibly compared between total intensity maps of different elements, for example, the near-white level in the autoscaled maps of Fig. 24.2 for Si, Fe, and Mn does not correspond to the same X-ray intensity or concentration for three elements. Because of autoscaling, it is not possible to compare maps for the same element "A" from two different regions, even if recorded with the same dose conditions, since the autoscaling factor will be controlled by the maximum concentration of "A," which may not be the same in two arbitrarily chosen regions of the sample.
3. This lack of quantitative information in elemental total intensity maps extends to the color overlay presentation of elemental maps seen in Fig. 24.2. The color overlay is useful to compare the spatial relationships among the three elements, but the specific color observed at any pixel only depicts elemental coincidence not absolute or relative concentration. The particular color that occurs at a given pixel depends on the complex physics of X-ray generation, propagation, and detection as well as concentration, and the autoscaling of the separate maps that precedes the color overlay, which distorts the apparent relationships among the elemental constituents, also influences the observed colors.
4. When peak interference occurs, the raw intensity in a given energy window may contain contributions from another element, as shown in Fig. 24.1 where the region that includes Fe K-$L_{2,3}$ also contains intensity from Mn K-$M_{2,3}$. While choosing the non-interfered peak Fe K-$M_{2,3}$ gives a useful result in the case of the manganese nodule, if the specimen also contained cobalt at a significant level, Co K-$L_{2,3}$ (6.930 keV) would interfere with Fe K-$M_{2,3}$ (7.057 keV) and invalidate this strategy. The peak interference artifact can be corrected by peak fitting, or by methods in which the measured Mn K-$L_{2,3}$ intensity, which does not suffer interference in this particular case, is used to correct the intensity of the Fe K-$L_{2,3}$ + Mn K-$M_{2,3}$ window using the known Mn K-$M_{2,3}$/K-$L_{2,3}$ ratio.
5. The total intensity window contains both the characteristic peak intensity that is specific to an element and the continuum (background) intensity, which scales with the average atomic number of all of the elements within the excited interaction volume but is not exclusively related to the element that is generating the peak. For the map of an element that constitutes a major constituent (mass concentration $C > 0.1$ or 10 wt %), the non-specific background intensity contribution usually does not constitute a serious mapping artifact. However, for a minor constituent ($0.01 \leq C \leq 0.1$, 1 wt % to 10 wt %), the average atomic number dependence of the continuum background can lead to serious artifacts. Figure 24.3 shows an example of this phenomenon for a Raney nickel alloy containing major Al and Ni with minor Fe. The complex microstructure has four distinct phases, the compositions of which are listed in Table 24.1, one of which contains Fe as a minor constituent at a concentration of approximately $C = 0.04$ (4 wt %). This Fe-rich phase can be readily discerned in the Fe gray-scale map, where the intensity of this phase, being the highest iron-containing region in the image, has been autoscaled to near white. In addition to this Fe-containing phase, there appears to be segregation of lower concentration levels of Fe to the Ni-rich phase relative to the Al-rich phase. However, this effect is at least partially due to the increase in the continuum background in the Ni-rich region relative to the Al-rich region because of the sharp difference in the average atomic number. For trace constituents ($C < 0.01$, 1 wt %), the atomic number dependence of the continuum background can dominate the observed contrast, creating artifacts in the images that render most trace constituent maps nearly useless.

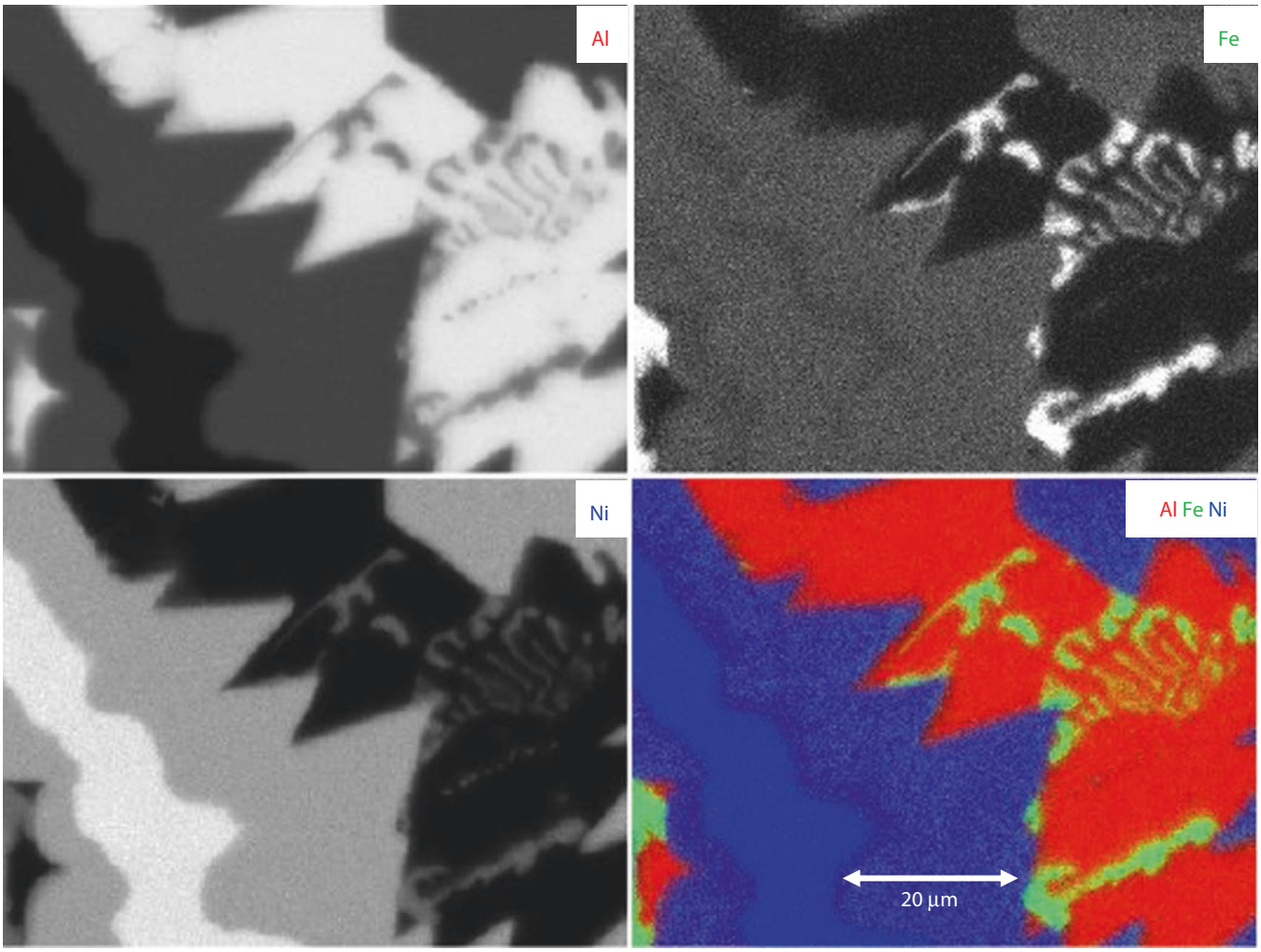

Fig. 24.3 Total intensity elemental maps for Al K-L_2 (major), Fe K-$L_{2,3}$ (minor), and Ni K-$L_{2,3}$ (major) measured on a cross section of a Raney nickel alloy, and the color overlay of the gray-scale maps

Table 24.1 Phases in Raney nickel; as measured by electron-excited X-ray microanalysis (mass concentrations)

	Al	Fe	Ni
High Al	0.995	0	0.005
Fe-rich	0.712	0.042	0.246
Intermediate Ni	0.600	0	0.400
High Ni	0.465	0	0.535

24.2 X-Ray Spectrum Imaging

X-ray spectrum imaging (XSI) involves collecting the entire EDS spectrum, I(E), at each pixel location, producing a large data structure [x, y, I(E)] typically referred to as a "datacube" (Gorlen et al. 1984; Newbury and Ritchie, 2013). Alternatively, the data may be recorded as "position-tagged" photons, whereby as each photon with energy E_p is detected, it is tagged with the current beam location (x, y), giving a database of values (x, y, E_p) which can be subsequently sampled with rules defining the range of Δx and Δy over which to construct a spectrum I(E) at a single pixel or over a defined range of pixels. Depending on the number of pixels and the intensity range of the X-ray count data, the recorded XSI can be very large, ranging from hundreds of megabytes to several gigabytes. Vendor software usually compresses the datacube to save mass storage space, but the resulting compressed datacube can only be decompressed and viewed with the vendor's proprietary software. As an important alternative, if the datacube can be saved in the uncompressed RAW format (a simple block of bytes with a header or an associated file that carries the metadata needed to read the file), the RAW file can be read by publically available, open source software such as NIH ImageJ-Fiji or NIST Lispix (Bright, 2017).

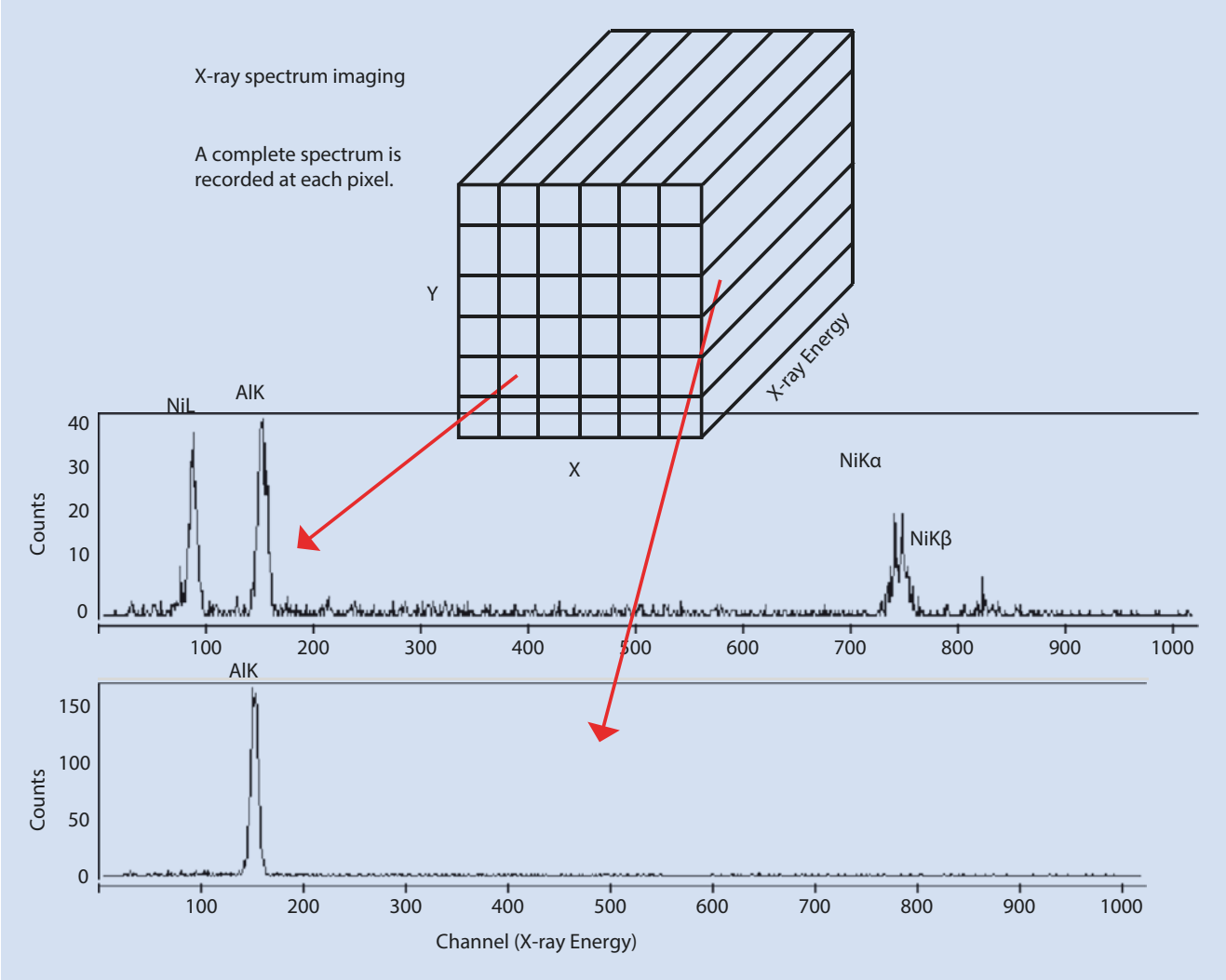

Fig. 24.4 X-ray spectrum image considered as a datacube of pixels x, y, I(E)

Regardless of how the measured photons are cataloged, the XSI captures all possible elemental information about the region of the specimen being mapped within the limitations set by the excitation energy (E_0), the dose (beam current multiplied by pixel dwell time, $i_B * \tau$), and the EDS spectrometer performance (solid angle and efficiency). Figure 24.4 shows the conceptual nature of the data. The [x, y, I(E)] datacube can be thought of as an x-y array of spectra I(E). The individual pixel spectra can be selected by the analyst for inspection by specifying the x-y location. Depending on the electron beam current, the pixel dwell time, and the solid angle of the EDS detector, the counts in an individual pixel spectrum may be low. For the example XSI of Raney nickel shown in Fig. 24.4, the upper spectrum taken from an Ni-rich area has a maximum of 40 counts per energy channel, while the lower spectrum from a different pixel in an Al-rich region has a maximum of 150 counts. An alternative view of the datacube is shown in Fig. 24.5, where the datacube can be thought of as a stack or deck of x-y image cards, where each x-y image corresponds to a different energy with an energy range ("card thickness") equal to the energy channel width, for example, typically 5 eV or 10 eV. If a card is selected from the stack with an energy that corresponds to a characteristic peak, then the card shows the elemental map for that peak, as shown in Fig. 24.5. A card with an energy that corresponds to spectral background will have fewer counts than a peak card, but such a background card may still have discernible microstructural information because of the atomic number dependence of the X-ray continuum, as shown in Fig. 24.5.

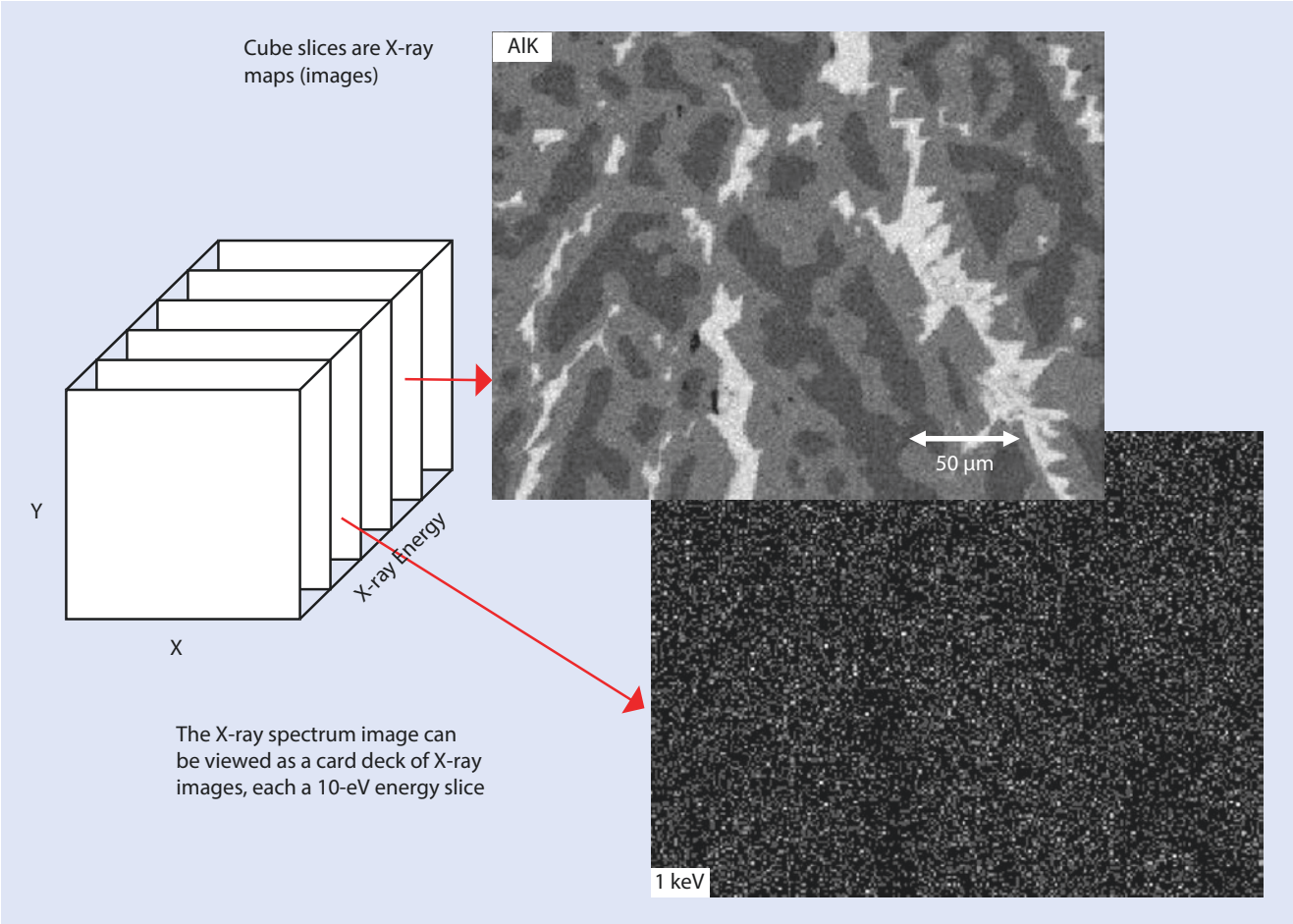

Fig. 24.5 X-ray spectrum image considered as a stack of x, y images, each corresponding to a specific photon energy E_p

24.2.1 Utilizing XSI Datacubes

In the simplest case, by capturing all possible X-ray information about an imaged region, the XSI permits the analyst to define regions-of-interest for total intensity mapping at any time after collecting the map datacube, creating elemental maps such as those in Fig. 24.2. If additional information is required about other elements not in the initial set-up, there is no need to relocate the specimen area and repeat the map since the full spectrum has been captured in the XSI.

The challenge to the analyst is to make efficient use of the XSI datacube by discovering ("mining") the useful information that it contains. Software for aiding the analyst in the interpretation of XSI datacubes ranges from simple tools in open source software to highly sophisticated, proprietary vendor software that utilizes statistical comparisons to automatically recognize spatial correlations among elements present in the specimen region that was mapped (Kotula et al. 2003).

24.2.2 Derived Spectra

SUM Spectrum

Simple but highly effective software tools that are present in nearly all vendor XSI platforms as well as the open source software (NIH ImageJ-Fiji and NIST Lispix) include those that calculate "derived spectra." Derived spectra are constructed by systematically applying an algorithm to the datacube to extract carefully defined information. The most basic derived spectrum is the "SUM" spectrum, illustrated schematically in Fig. 24.6. Conceptually, each energy "card" in the XSI datacube is selected and the counts in all pixels on that card are added together, as indicated by the systematic route through all pixels shown in Fig. 24.6. This summed count value is then placed in the corresponding energy bin of the SUM spectrum under construction, and the process is then repeated for the next energy card until all energies have been considered. The resulting SUM spectrum has the familiar features of a conventional spectrum: characteristic X-ray peaks and the

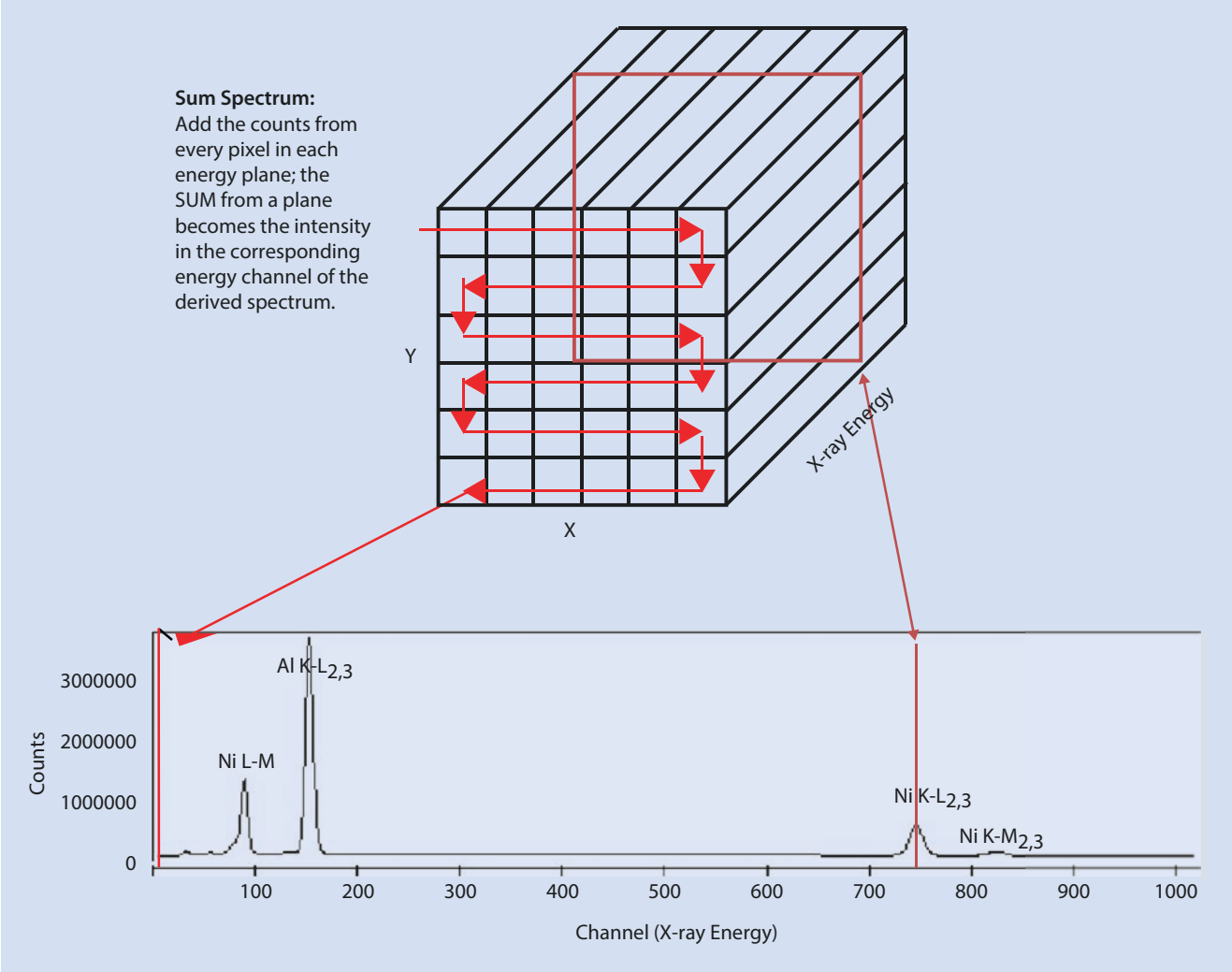

Fig. 24.6 Concept of the SUM spectrum derived from an X-ray spectrum image by adding the counts from all pixels on an individual image at a specific photon energy, E_p

X-ray continuum background, as well as artifacts such as coincidence peaks and Si-escape peaks. The SUM spectrum in Fig. 24.6 was calculated from the same Raney nickel XSI datacube used for Fig. 24.4. Note that the count axis now extends to more than 3 million counts, much higher than the count axes of the individual pixel spectra in Fig. 24.4 because of the large number of pixels that have been added together to construct the SUM spectrum. The characteristic peaks that can be recognized in the SUM spectrum (scaled to the highest intensity) represent the dominant, most abundant elemental features contained in the XSI. The analyst can select a peak channel and view the corresponding energy card to reveal the elemental map for that peak, as shown in Fig. 24.7. By selecting a band of adjacent channels that spans the peak and averaging the counts for each x-y pixel in the set of energy cards, an elemental image with reduced noise is obtained, as also shown in Fig. 24.7. Systematically selecting each of the prominent characteristic X-ray peaks, total intensity maps for all of the major elemental constituents can be obtained. The SUM spectrum can be treated just like a normally recorded spectrum. By expanding the vertical scale or changing from a linear display to a logarithmic display, lower relative intensity

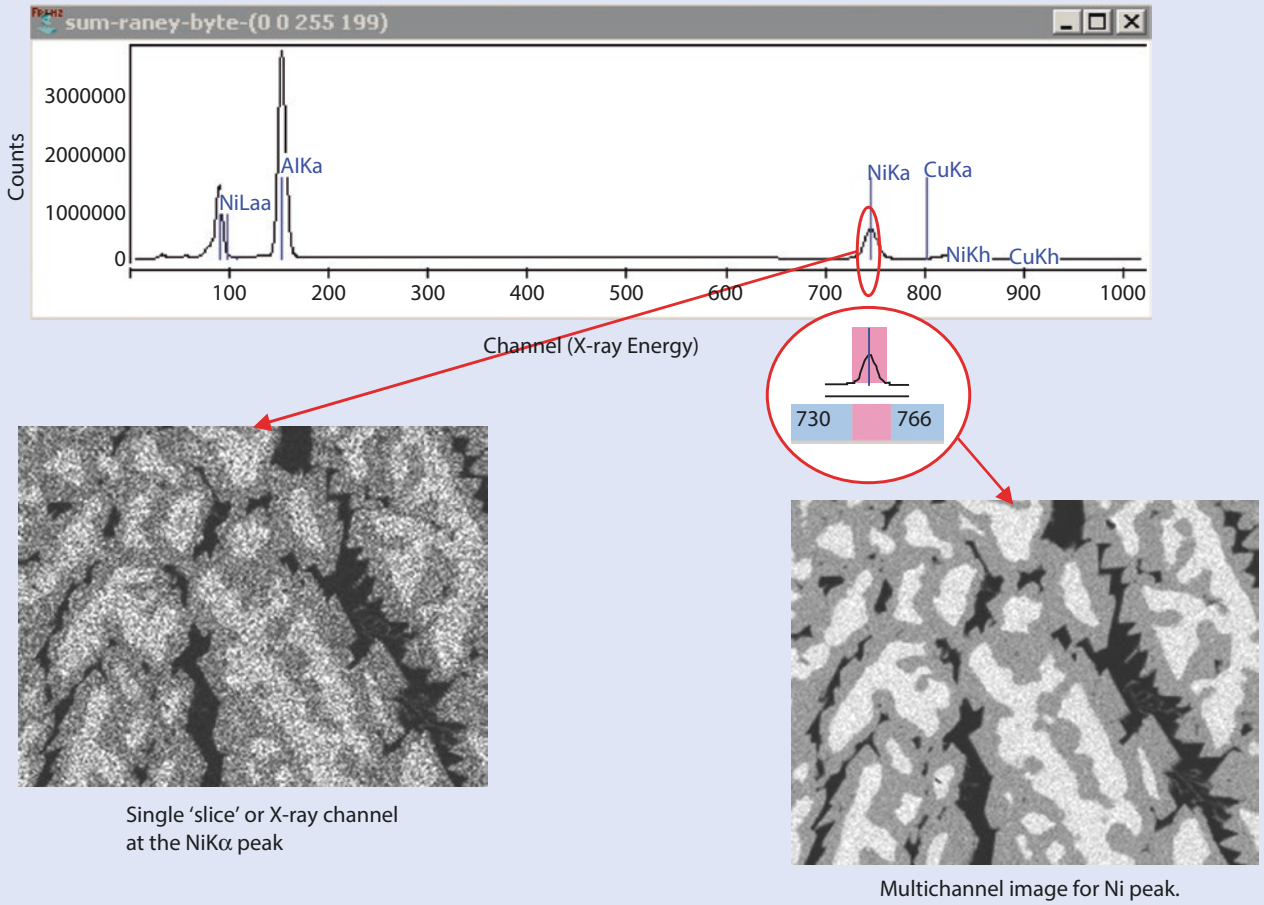

Fig. 24.7 Using the SUM spectrum to interrogate an X-ray spectrum image to find the dominant elemental peaks for the region being mapped

peaks corresponding to minor and trace constituents can be recognized, and the corresponding total-intensity region-of-interest images can be constructed, subject to the increasing influence of the continuum background incorporated in the window. For these lower abundance constituents, it is necessary to use a band of energy channels to reduce the noise in the resulting elemental image, and such images are subject to the artifacts that arise from the atomic number dependence of the X-ray continuum noted above.

MAXIMUM PIXEL Spectrum

The SUM spectrum reveals dominant elemental features in the mapped region. Rare, unexpected elemental features, which in the extreme case may occur at only a single pixel (i.e., looking for a "needle-in-a-haystack" when you don't even know that it is a needle you are looking for!) can be recognized with the "MAXIMUM PIXEL" derived spectrum (Bright and Newbury 2004). As shown in Fig. 24.8, the MAXIMUM PIXEL derived spectrum is calculated by making the same tour through all of the pixels on each energy card as is done for the SUM spectrum, but rather than adding the pixel contents, the algorithm now locates the maximum intensity within a card regardless of what pixel it comes from to represent that energy value in the constructed MAXIMUM PIXEL spectrum. An example of the application of the MAXIMUM PIXEL spectrum to an XSI is shown in Fig. 24.9, where an unanticipated Cr peak is recognized. When the Cr image is selected from the XSI, the Cr is seen to be localized in a small cluster of pixels. Note that in the plot of the SUM, LOG_{10}SUM, and MAXIMUM PIXEL spectra in Fig. 24.9, the Cr peak is only visible in the MAXIMUM

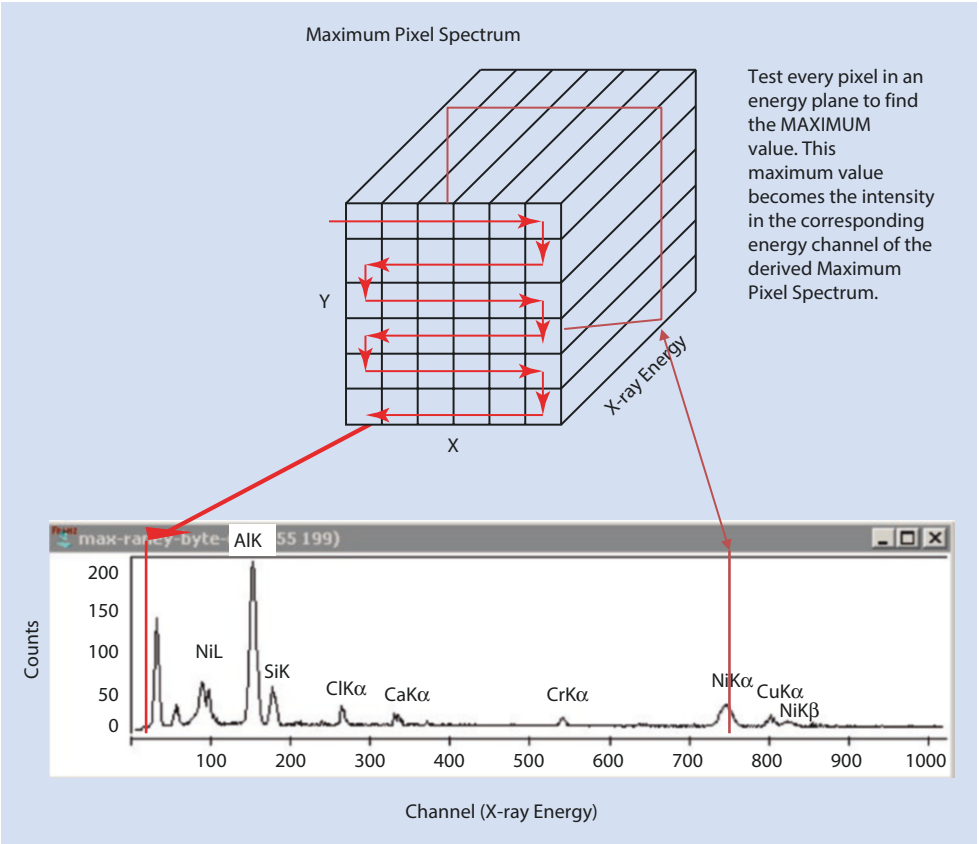

Fig. 24.8 Concept of the MAXIMUM PIXEL spectrum derived from an X-ray spectrum image by finding the highest count among all the pixels on an individual image at a specific photon energy, E_p

PIXEL spectrum. Because Cr is represented at only a few pixels, in the SUM spectrum the Cr intensity is overwhelmed by the continuum intensity at all of the other pixels, so that the Cr peak is not visible even in the logarithmic expansion shown in the LOG_{10}SUM plot.

After the elemental maps have been created from the XSI, additional image processing tools can be brought to bear. Spatial regions-of-interest can be defined in the elemental maps or in corresponding BSE or SE images recorded simultaneously with the XSI. These spatial regions can be selected by simple image processing tools that define a group of contiguous pixels that fall within a particular shape (square, rectangle, circle, ellipsoid, or closed free form are typical choices). Another approach is the creation of a pixel mask by selecting all pixels within a particular elemental map (or BSE or SE image) whose intensities fall within a defined range above a specified gray level threshold. Pixels that satisfy this intensity criterion can occur anywhere in the x–y plane of the XSI and do not have to be contiguous. Selections can range down to an individual pixel. An example of this process is shown in Figure 24.10, where the Fe-rich phase has been selected from the Fe total intensity map (shown in color overlay with Al and Ni) to create a mask (shown as a binary image in the inset) from which the SUM spectrum representing the Fe-rich phase is constructed.

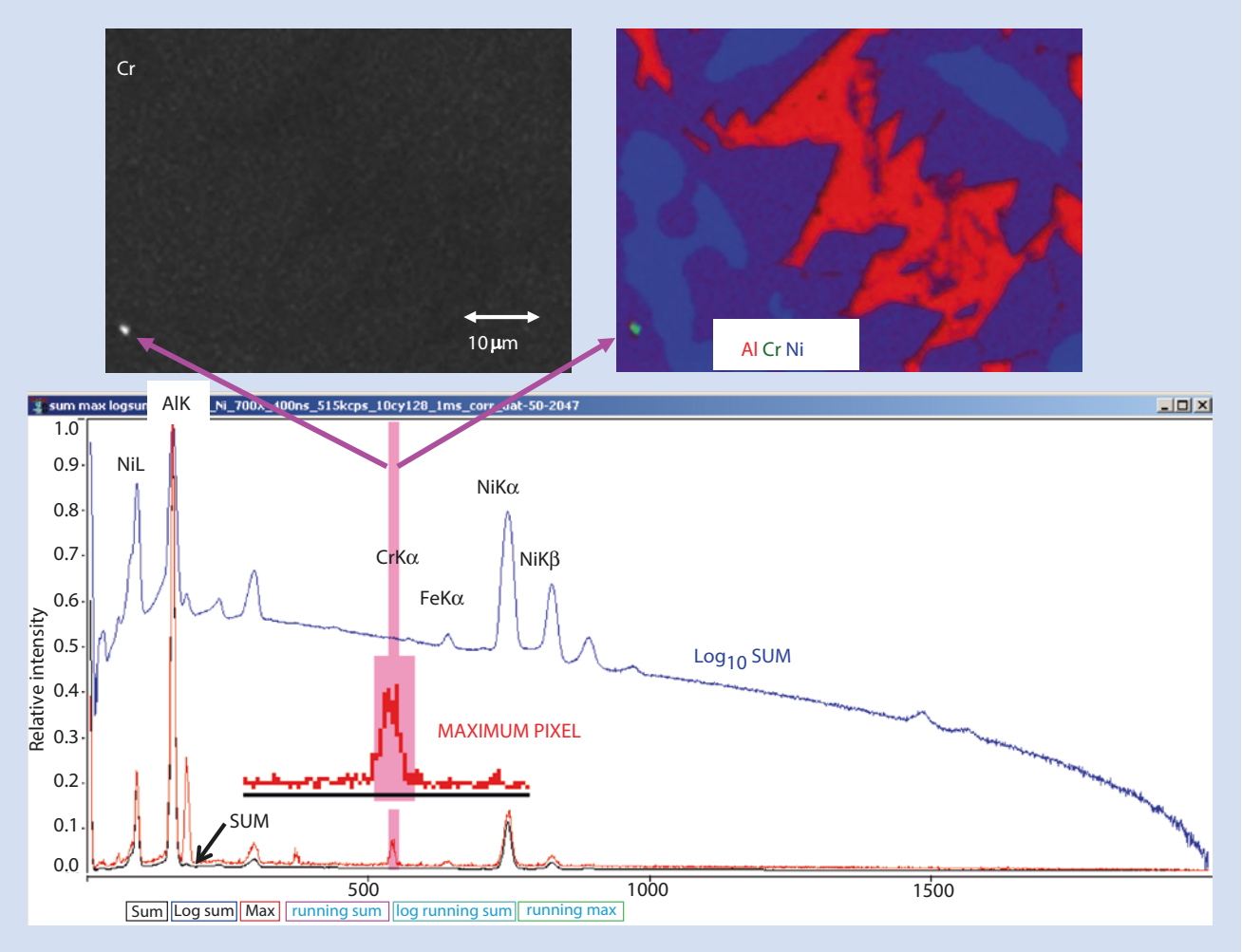

Fig. 24.9 Use of the MAXIMUM PIXEL spectrum to identify and locate an unexpected Cr-rich inclusion in Raney nickel alloy

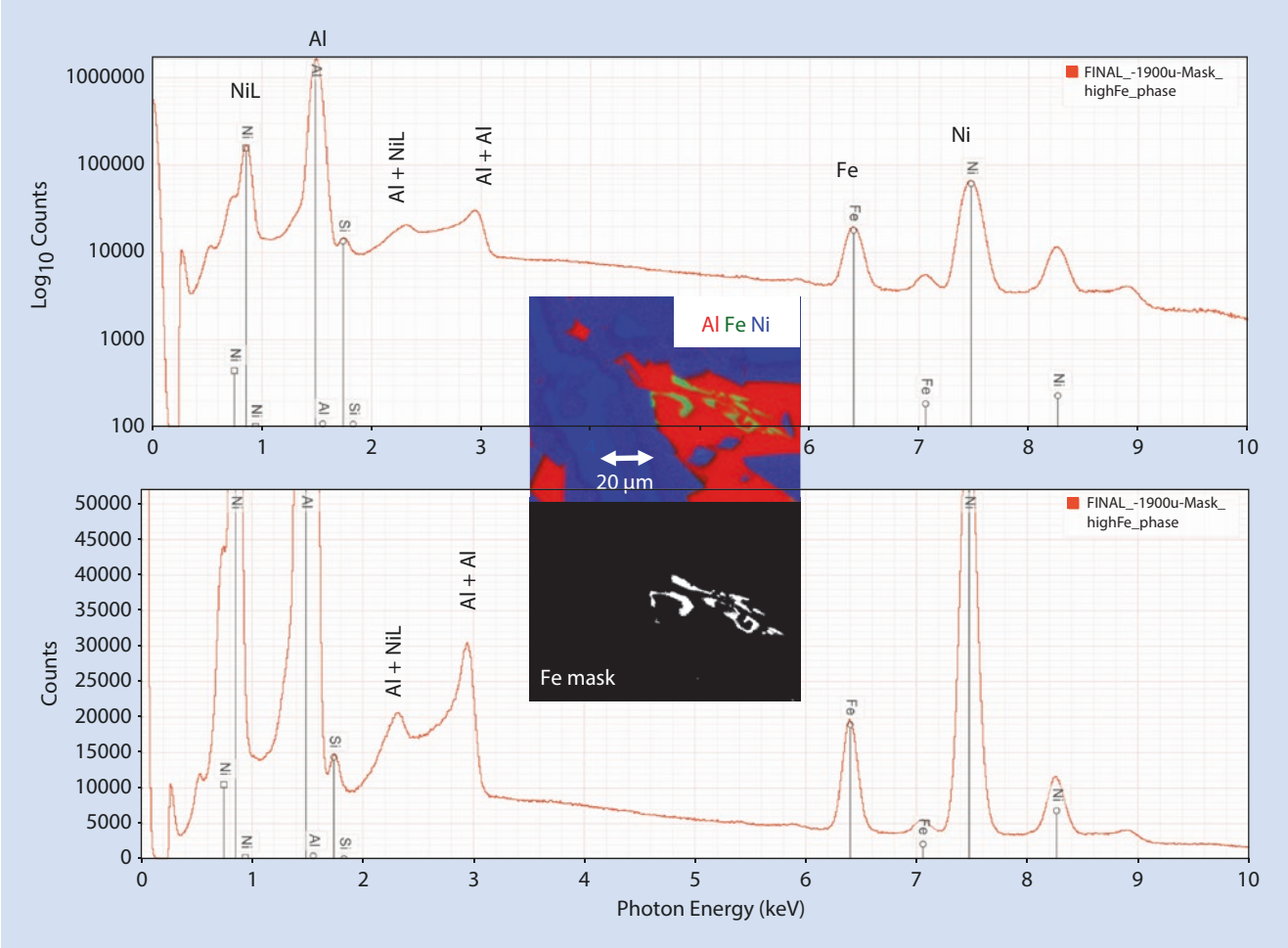

Fig. 24.10 Creation of a pixel mask (inset) using the Fe elemental map for Raney nickel to select pixels from which a SUM spectrum is constructed for the Fe-rich phase

24.3 Quantitative Compositional Mapping

The XSI contains the complete EDS spectrum at each pixel (or the position-tagged photon database that can be used to reconstruct the individual pixel spectra). Quantitative compositional mapping implements the normal fixed measurement location quantitative analysis procedure at every pixel in a map. Qualitative analysis is first performed to identify the peaks in the SUM and MAXIMUM PIXEL spectra of the XSI to determine the suite of elements present within the mapped area, noting that all elements are unlikely to be present at every pixel. The pixel-level EDS spectra can then be individually processed following the same quantitative analysis protocol used for individually measured spectra, ultimately replacing the gray or color scale in total intensity elemental maps, which are based on raw X-ray intensities and which are nearly impossible to compare, with a gray or color scale based on the calculated concentrations, which can be sensibly compared. Most vendor compositional mapping software extracts characteristic peak intensities by applying multiple linear least squares (MLLS) peak fitting or alternatively fits a background model under the peaks. These extracted pixel-level elemental intensities are then quantified by a "standardless analysis" procedure to calculate the individual pixel concentration values. Alternatively, rigorous standards-based quantitative analysis can be performed on the pixel-level intensity data with NIST DTSA II by utilizing the scripting language to sequentially calculate the pixel spectra in a datacube. MLLS peak fitting to extract the characteristic intensities, k-ratio calculation relative to a library of measured standards, and matrix corrections to yield the local concentrations of these elements for each pixel. An example of the NIST DTSA-II procedure applied to an XSI measured on the manganese nodule example of Fig. 24.2 is presented in Fig. 24.11, where the Fe K-$L_{2,3}$ total intensity map, which suffers significant interference from Mn K-$M_{2,3}$, shows a change in the apparent level of Fe in the center of the image after quantitative correction, as well as changes in several finer-scale details.

Quantitative compositional maps for major constituents displayed as gray-scale images are virtually identical to raw intensity elemental maps, as shown for the major constituents Al and Ni in Figs. 24.12 and 24.13. Significant differences between raw intensity maps and compositional maps are found for minor and trace constituents, where correction

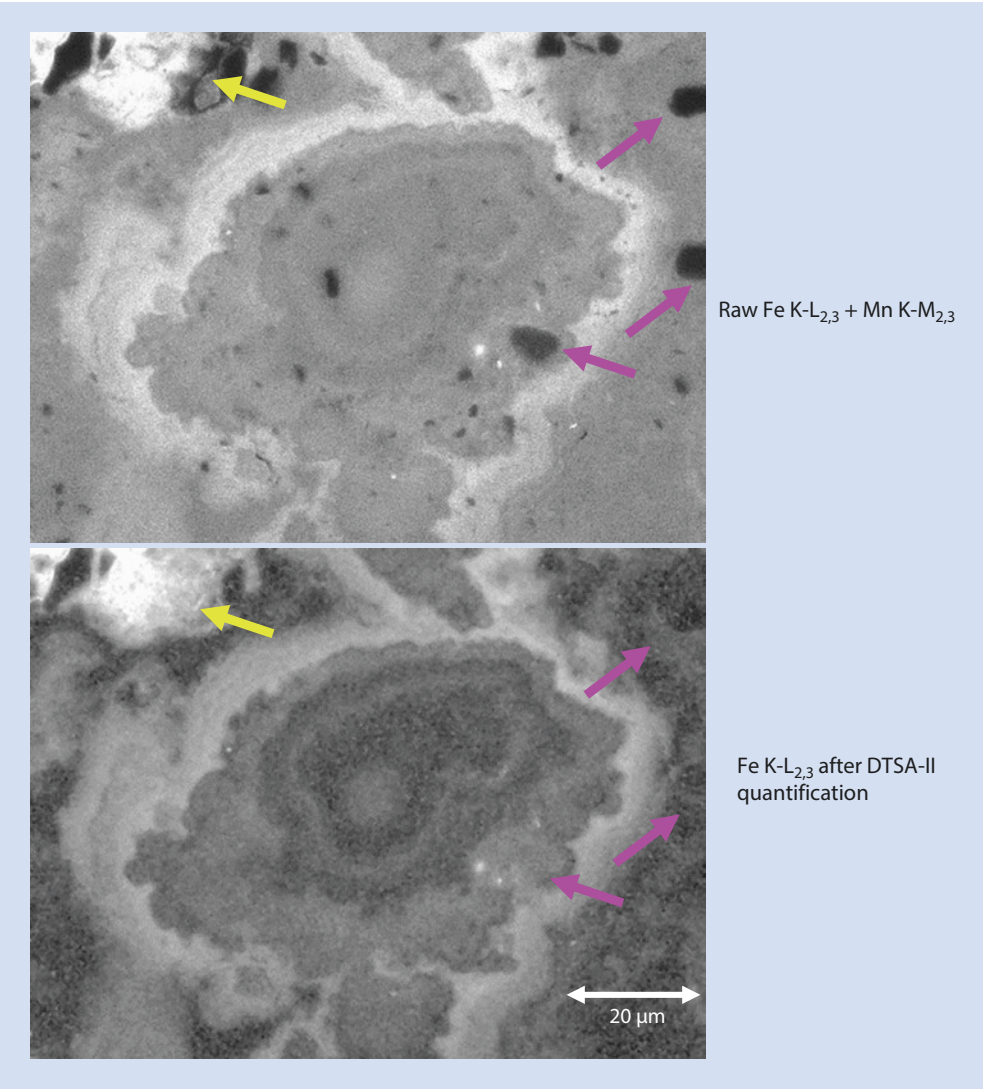

Fig. 24.11 Quantitative compositional mapping with DTSA-II on the XSI of a deep-sea manganese nodule from Fig. 24.2: direct comparison of the total intensity map for Fe and the quantitative compositional map of Fe; note the decrease in the apparent Fe in the high Mn portion in the center of the image after quantification and local changes indicated by *arrows* (*yellow* shows extension of high Fe region; magenta shows elimination of *dark* features)

for the continuum background significantly changes the gray-scale image. As shown for the minor Fe constituent in Figs. 24.12 and 24.13, the false Fe contrast between the Ni-rich and Al-rich phases that arises due to the atomic number dependence of the X-ray continuum is eliminated in the Fe compositional map.

While rendering the underlying pixel data of quantitative compositional maps in gray scale is a useful starting point, the problem of achieving a quantitatively meaningful display remains. Because of autoscaling, the gray scales of the Al, Ni, and Fe maps in Fig. 24.12 do not have the same numerical meaning. The Al and Ni concentrations locally reach high enough levels to correspond to brighter gray levels and have sufficient range to create strong contrast with direct gray-scale encoding, as seen in Figs. 24.12 and 24.13. The Fe constituent which is present at a concentration with a maximum of approximately 0.04 mass fraction (4 wt %) never exceeds the minor constituent range, so the Fe map appears dark with little contrast in the quantitative map of Fig. 24.13. Autoscaling of the Fe-map in Fig. 24.14 improves the contrast, but the same limitations of autoscaling noted above still apply. Various pseudo-color scales, in which bands of contrasting colors are applied to the underlying data, are typically available in image processing software. Such pseudo-color scale can partially overcome the display limitations of gray-scale presentation, but the resulting images are often difficult to interpret. An example of a five band pseudo-color scale applied to the compositional maps using NIST Lispix is shown in Fig. 24.15. An effective display scheme for quantitative elemental maps that enables a viewer to readily compare concentrations of different elements spanning major, minor and trace ranges can be achieved with the Logarithmic Three-Band Encoding (Newbury and Bright 1999). A band of colors is assigned to each decade of the concentration range with the following characteristics:

Major: $C > 0.1$ to 1 (mass fraction) deep red to red pastel
Minor: $0.01 \leq C \leq 0.1$ deep green to green pastel
Trace: $0.001 \leq C < 0.01$ deep blue to blue pastel

The quantitative elemental maps are displayed with Logarithmic Three-Band Encoding in Fig. 24.16, and the

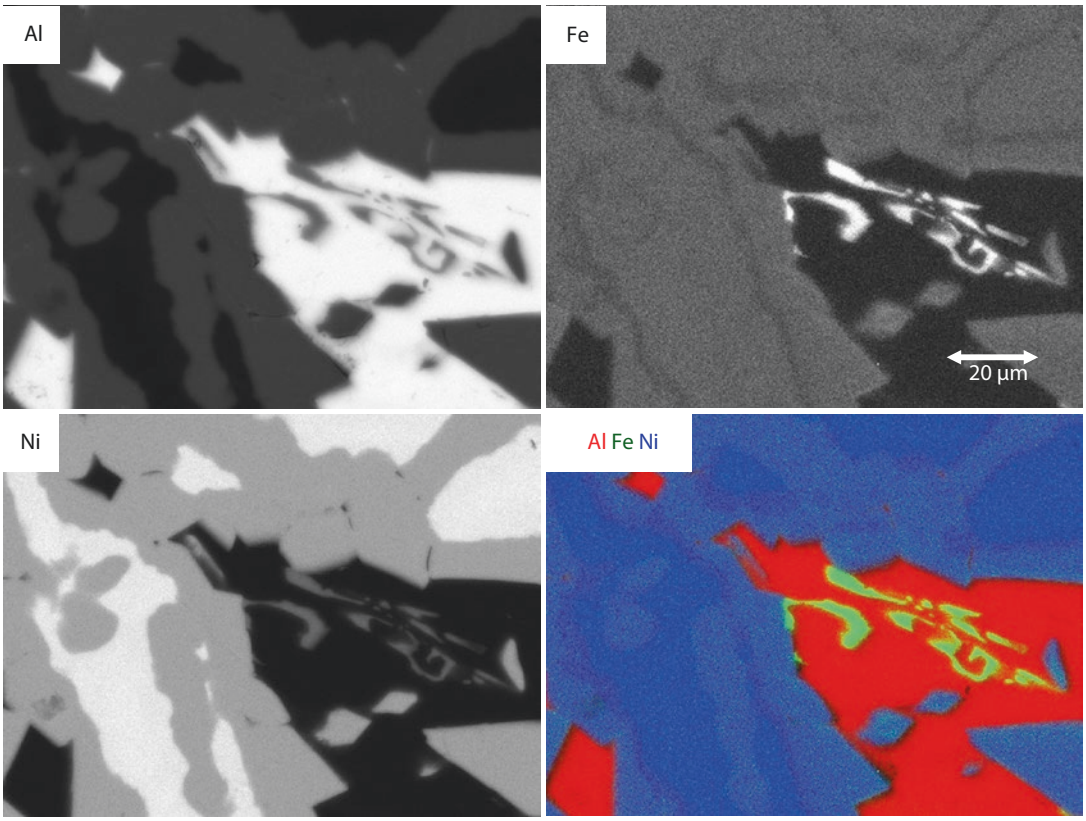

Fig. 24.12 Raney nickel alloy XSI: total intensity maps for Al, Fe, and Ni with color overlay

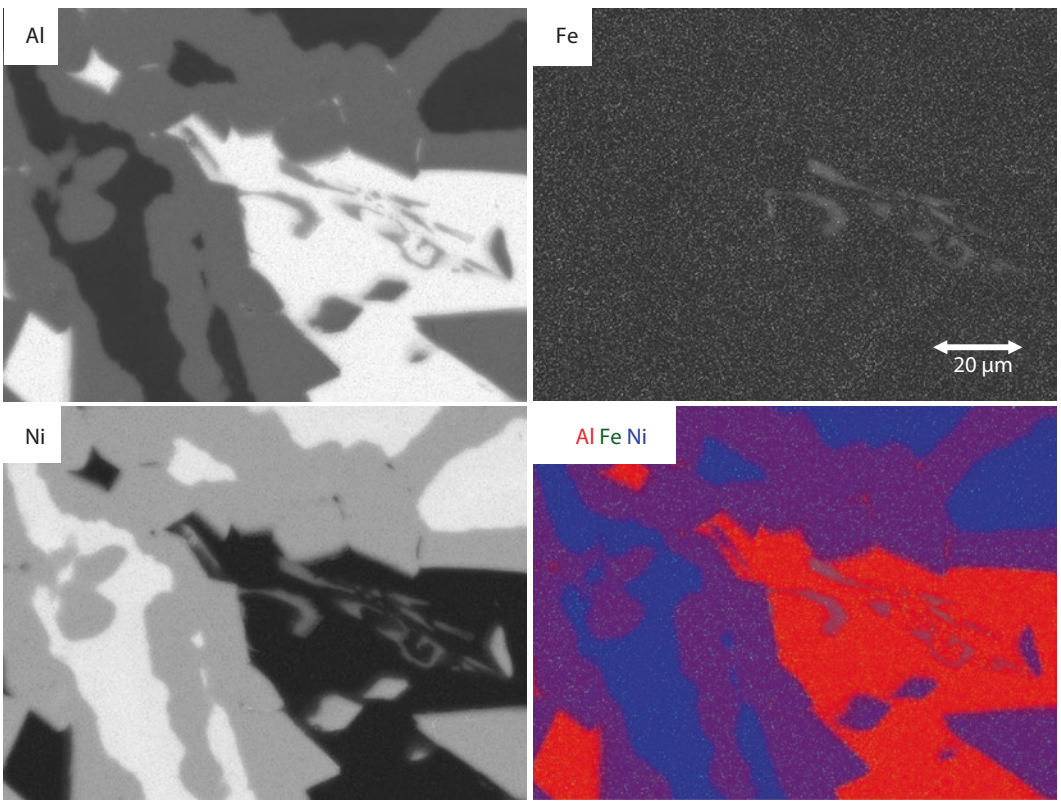

Fig. 24.13 Quantitative compositional maps of the Raney nickel alloy XSI in 24.13; note low contrast in the Fe image presented without autoscaling

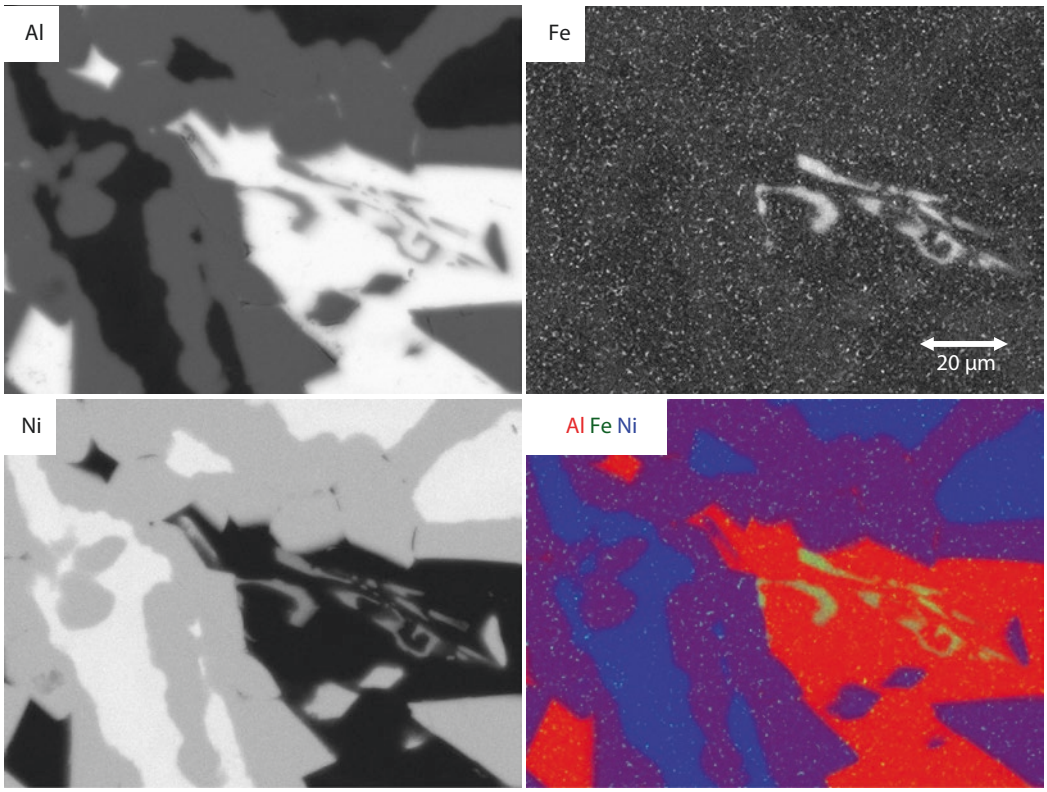

Fig. 24.14 Quantitative compositional maps Raney nickel alloy XSI with contrast enhancement of the Fe map

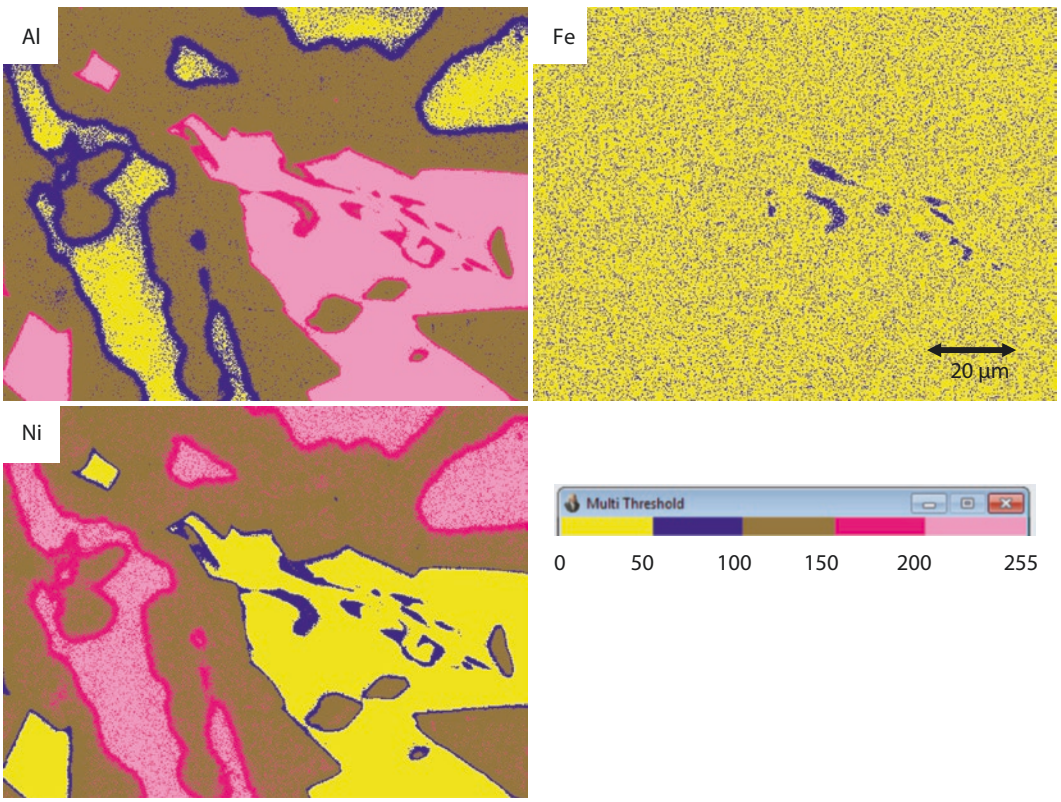

Fig. 24.15 Five band pseudo-color presentation of the quantitative compositional maps for Al, Fe, and Ni derived from the Raney nickel alloy XSI

major-minor-trace spatial relationships among the elemental constituents are readily discernible.

The Logarithmic Three-Band Encoding of the Fe compositional map in Fig. 24.16 reveals apparent Fe contrast in the Al-rich and Fe-rich phases, and this contrast differs markedly from the atomic-number dependence of the X-ray continuum seen in the raw Fe intensity image, as shown in Fig. 24.17. The Logarithmic Three-Band Encoding shows that this apparent contrast occurs near the lower limit of the trace range. Is this trace Fe contrast meaningful or merely an uncorrected

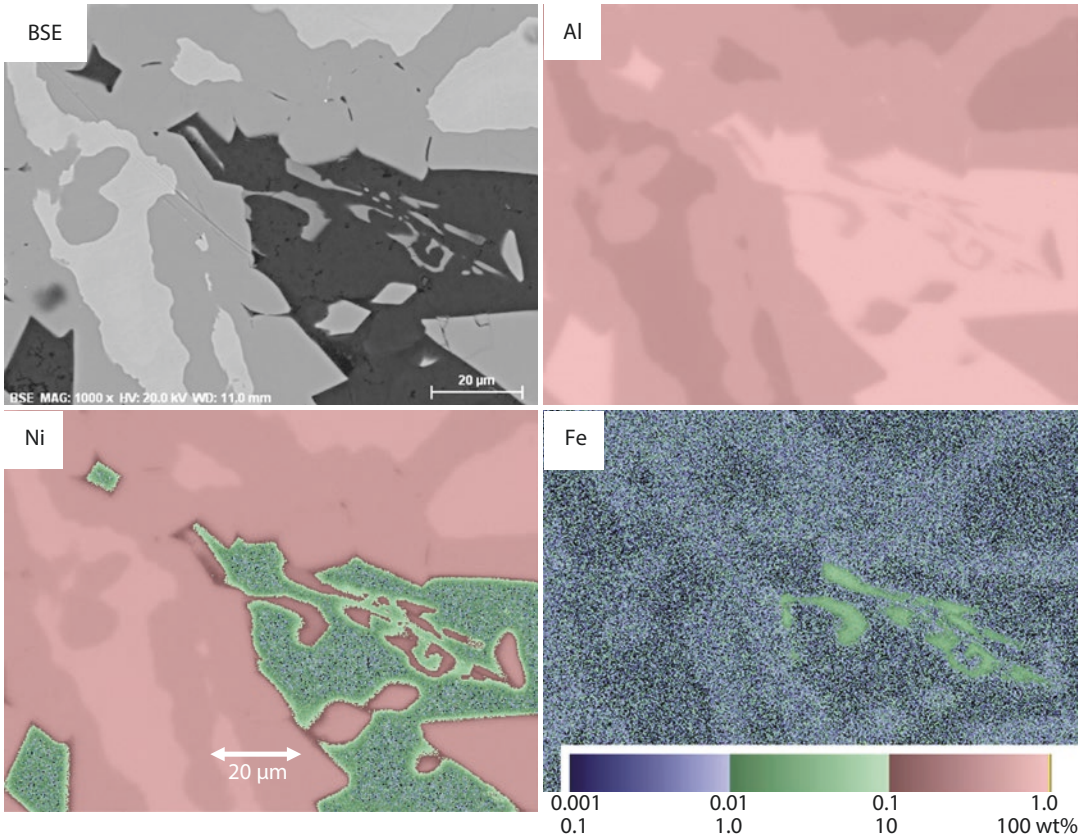

Fig. 24.16 Logarithmic Three-Band Color encoding of the quantitative compositional maps for Al, Fe, and Ni derived from the Raney nickel alloy XSI

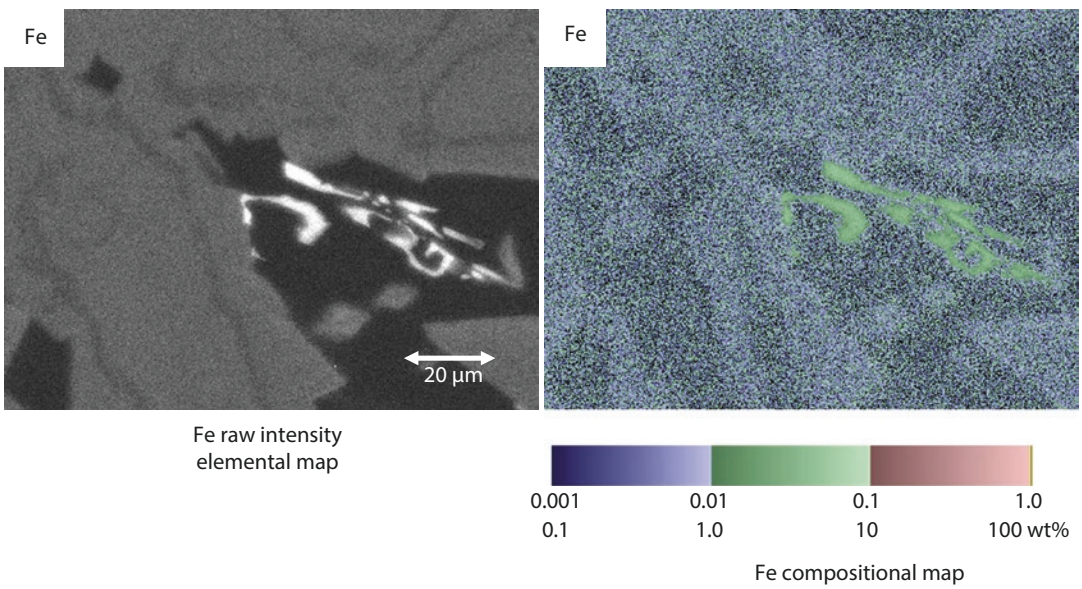

Fig. 24.17 Direct comparison of the Fe total intensity map and the Logarithmic Three-Band Encoding of the Fe quantitative compositional map. Note the distinct changes in the contrast within the trace concentration ($C < 0.01$) regions of the image

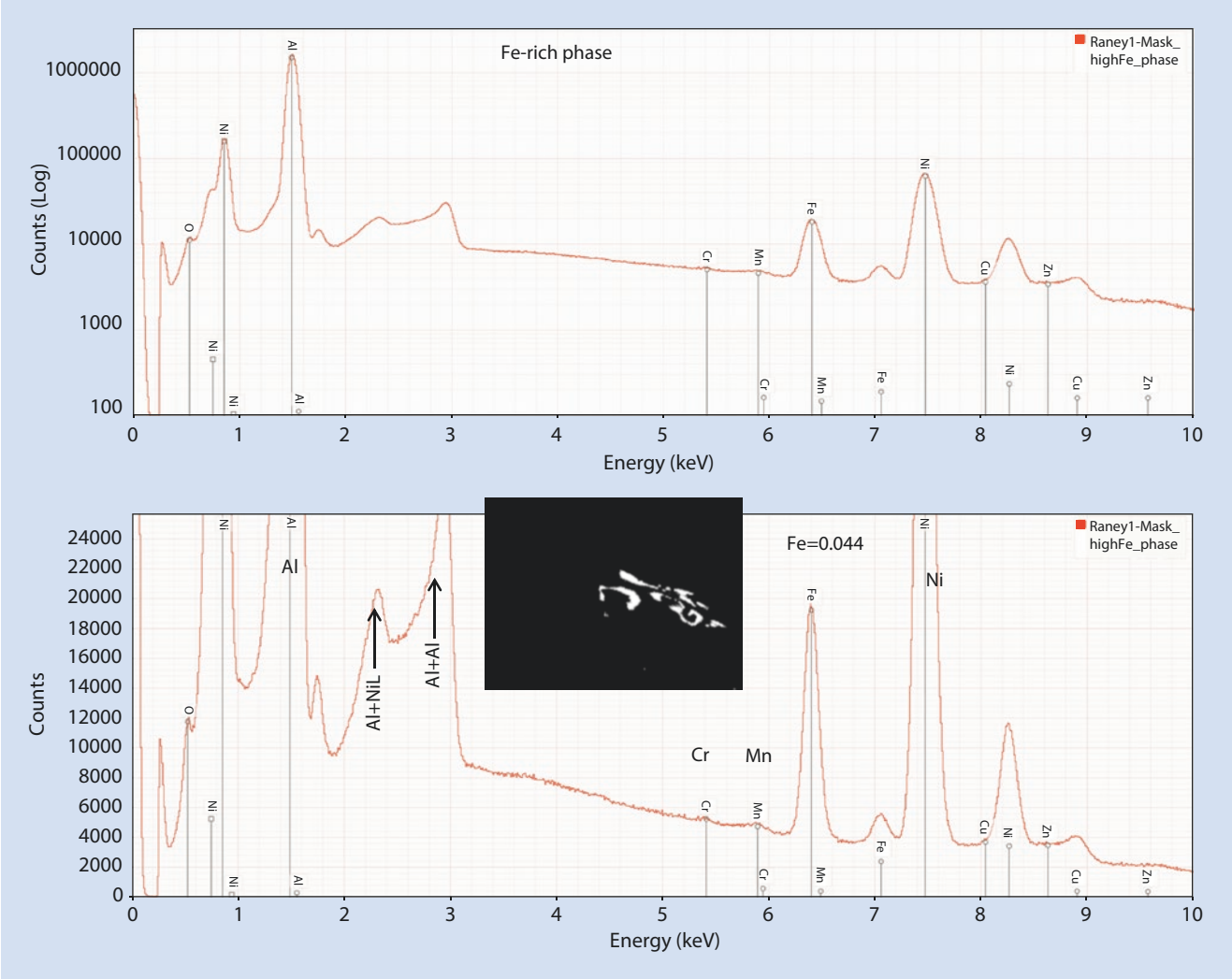

Fig. 24.18 Raney nickel alloy XSI: mask of pixels corresponding to the Fe-rich phase and the corresponding SUM spectrum; the Fe peak corresponds to $C = 0.044$ mass fraction

artifact? To examine this question, the analyst can use pixel masks of each phase selected from the Ni compositional map (or the BSE image) to obtain the SUM spectrum, as shown in Figs. 24.18 (Fe-rich phase), 24.19 (Al-rich phase), 24.20 (Ni-intermediate phase), and 24.21 (Ni-rich phase). These SUM spectra confirm that Fe is indeed present as a trace constituent, with its highest level in the intermediate-Ni phase where $C_{Fe} = 0.0027$ (2700 ppm), falling to $C_{Fe} = 0.00038$ (380 ppm) in the high-Ni phase and to $C_{Fe} = 0.00030$ (300 ppm) in the high-Al phase. Additionally, trace Cr at a similar concentration is found in the Al-rich phase along with the trace Fe.

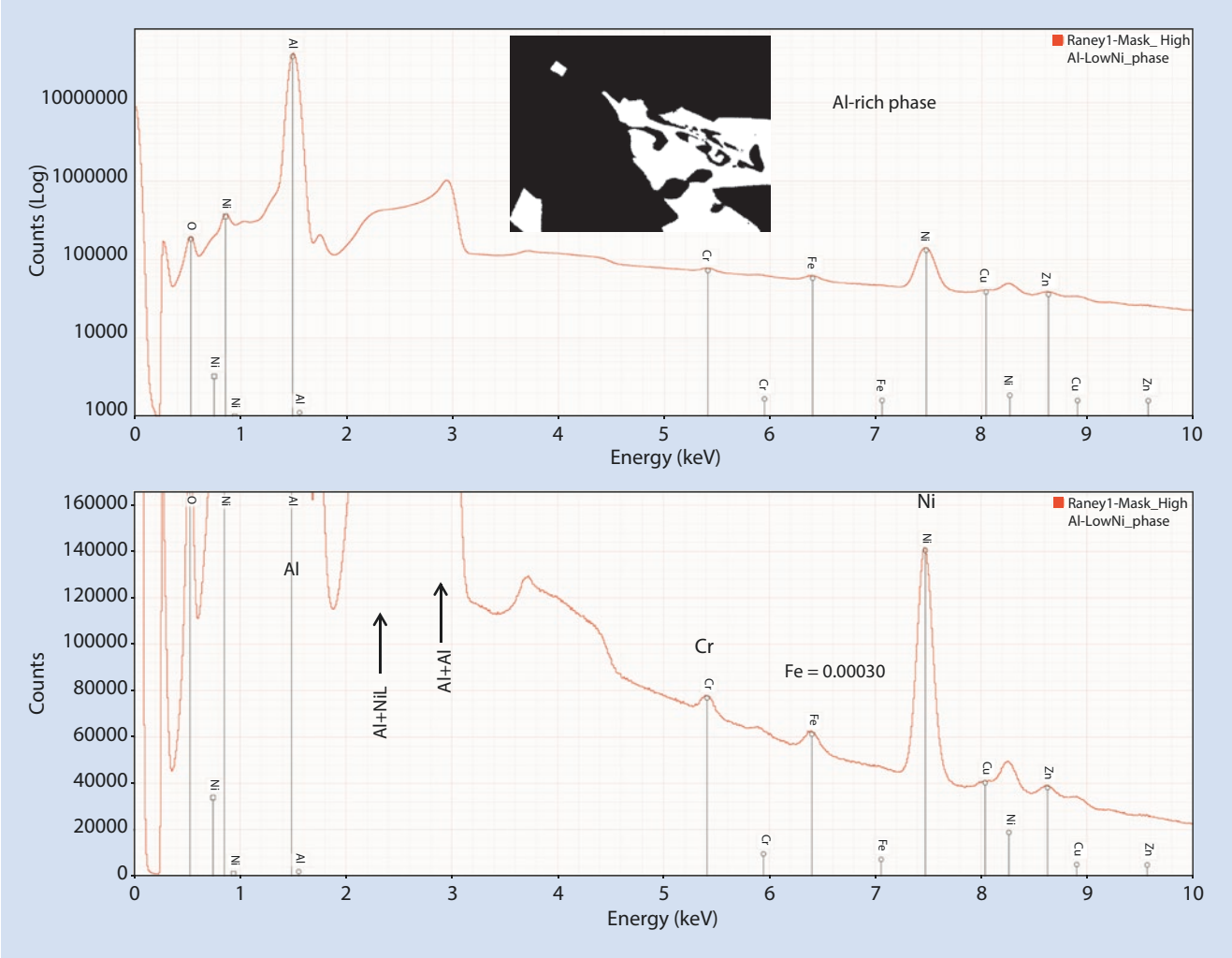

Fig. 24.19 Raney nickel alloy XSI: mask of pixels corresponding to the Al-rich phase and the corresponding SUM spectrum; note the low level peaks for Fe and Cr; the Fe-peak corresponds to $C = 0.00030 = 300$ parts per million

24.4 Strategy for XSI Elemental Mapping Data Collection

24.4.1 Choosing the EDS Dead-Time

The analyst has a choice of time constants in the EDS software, a parameter variously known as shaping time, processing time, etc., and typically expressed as time value (e.g., 200 ns, 400 ns, 1 µs), as a count rate value (e.g., the throughput at the peak of the input–output response), or as a simple integer. The shorter the time constant, the higher the peak throughput, expressed as the output count rate (OCR) versus the input count rate (ICR), but the poorer the resolution. The performance of a silicon drift detector (SDD)-EDS with three time constant choices is illustrated in Fig. 24.22, where the peak of the OCR vs. ICR plot varies dramatically with the time constant selected. All forms of EDS microanalysis are improved by increasing the number of X-ray counts measured, but elemental mapping is especially dependent on accumulating large numbers of X-rays since mapping divides the total count among a large number of pixels. To obtain adequate counts per pixel for meaningful analytical information at the individual pixel level, it is common practice to accept the resolution penalty to operate on the highest throughput curve in Fig. 24.22. Of course, to produce the X-ray flux necessary to make use of this throughput capability, the EDS detector solid angle should first be maximized by operating at the shortest specimen-to-EDS distance (for a movable EDS) and the beam current should then be adjusted accordingly to produce an acceptable dead-time. An

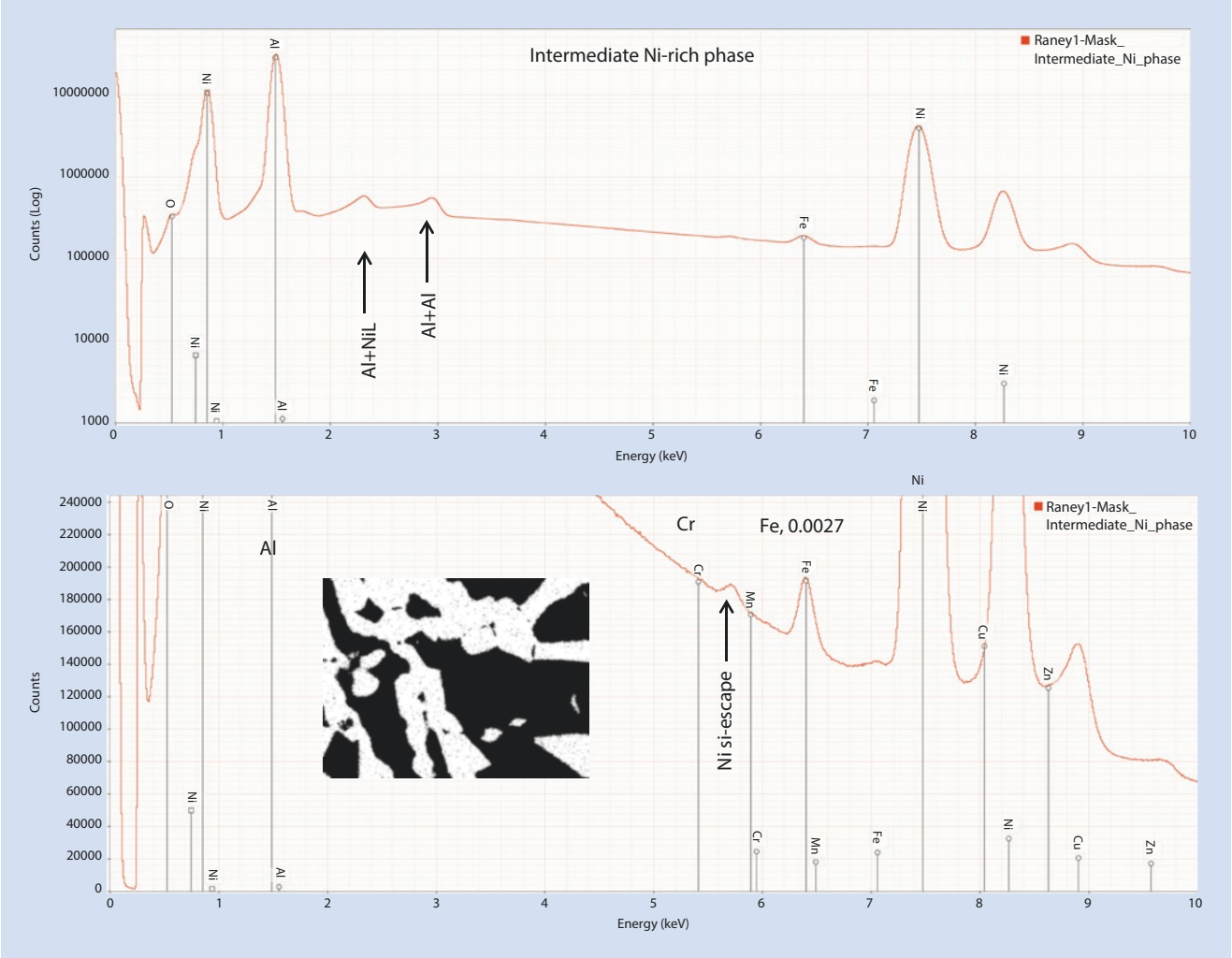

Fig. 24.20 Raney nickel alloy XSI: mask of pixels corresponding to the intermediate Ni-rich phase and the corresponding SUM spectrum; note the low level peak for Fe; the Fe-peak corresponds to $C = 0.0027 = 2700$ parts per million

acceptable dead-time will depend on the level of spectral artifacts that the analyst is willing to accept: (1) If the mapping software collects the XSI at constant pixel dwell time without dead-time correction, the resulting map can be subject to severe artifacts if the dead-time is so high that the peak of the OCR versus ICR response is exceeded at some pixels during mapping. As shown in Fig. 24.23, operating at very high dead-time can result in the same OCR being produced by two widely different ICR values, which may effectively correspond to two different concentrations. Artifacts produced by this effect are shown in the Al elemental maps recorded at high dead-time shown in Fig. 24.24. Dead-time-corrected data collection in elemental mapping avoids this artifact. (2) If the analyst is interested in minor and/or trace level constituents, coincidence artifacts, which scale with dead-time, must be considered. Coincidence peaks for Al + NiL and Al + Al, as well as the coincidence continuum between these peaks, are illustrated in Figs. 24.18, 24.19, 24.20, and 24.21. This portion of the EDS spectrum contains K-shell peaks for S and Cl, L-shell peaks for Mo, Tc, Ru, Rh, Pd, and Ag, and M-shell peaks for Hg, Tl, Pb, and Bi. If none of these elements is of interest at the minor or trace level, then the Al + NiL and Al + Al coincidence can be ignored and the advantages of high throughput realized for the other elements of interest. However, if this spectral region is required for one or more of these elements, a lower dead-time should be selected by reducing the beam current to reduce coincidence, which depends strongly on the input count rate.

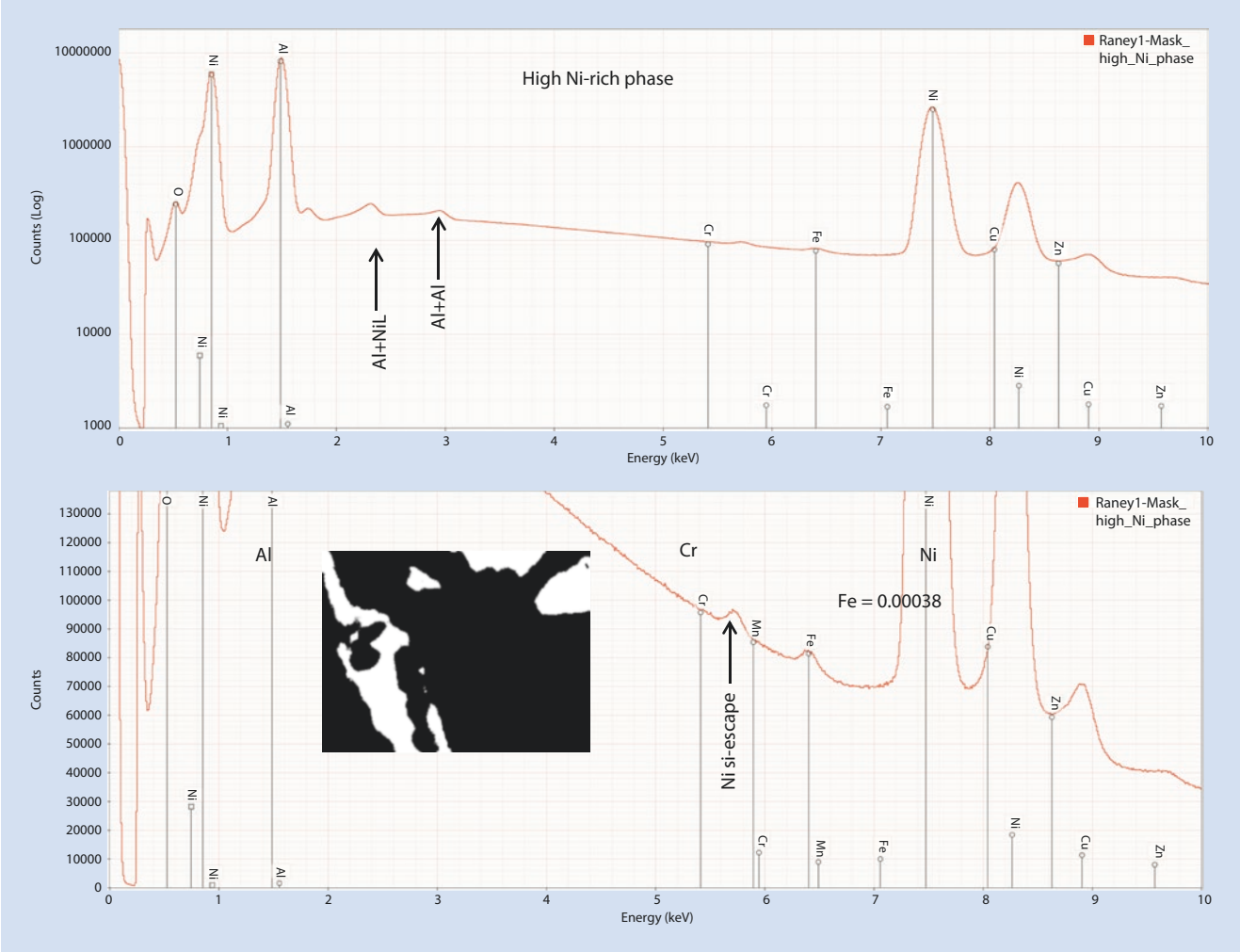

Fig. 24.21 Raney nickel alloy XSI: mask of pixels corresponding to the high Ni-rich phase and the corresponding SUM spectrum; note the low level peak for Fe; the Fe-peak corresponds to $C = 0.00038 = 380$ parts per million

24.4.2 Choosing the Pixel Density

The size of the scanned area, the number of image pixels (n_X, n_Y) and the pixel dwell time, τ, are critical parameters that the analyst must choose when defining an XSI data collection. An estimate of the size of the lateral extent of the X-ray interaction volume, obtained either from the Kanaya–Okayama X-ray range or from Monte Carlo simulation, is also useful, especially for small-area, high-magnification mapping. Choosing the size of the scanned area (magnification) depends on the lateral extent of the specimen features that are the objective of the mapping measurement. As is the case with SEM imaging using BSEs and/or SEs, when large areas are being scanned (low magnification operation), the pixel size may be greater than the lateral extent of the X-ray source size, which is a convolution of the incident beam size and the interaction volume for X-ray production, so that much of the pixel area is effectively unsampled. In principle, the empty area of the pixel could be "filled in" by increasing the number of pixels to reduce the pixel size, but this would lead to extremely large XSI data structures that would require very long accumulation times. A practical upper limit for XSI mapping is typically 1024×1024 pixels, which for a spectrum of 4096 channels of 2 bytes intensity depth would produce an XSI of 8 Gbytes in the uncompressed RAW format. To reduce the mass storage as well as the subsequent processing time for quantitative compositional mapping calculations, the analyst may choose 512×512 or 256×256 pixel scan fields, especially when a small area is scanned (high magnification operation) leading to overlapping pixels. A pixel overlap of approximately 25 % serves to fill all space in the square pixels, but further oversampling provides no additional information, so that the analyst would be better served by lowering the magnification to cover more specimen area with the chosen pixel density, or alternatively, choose a lower pixel density.

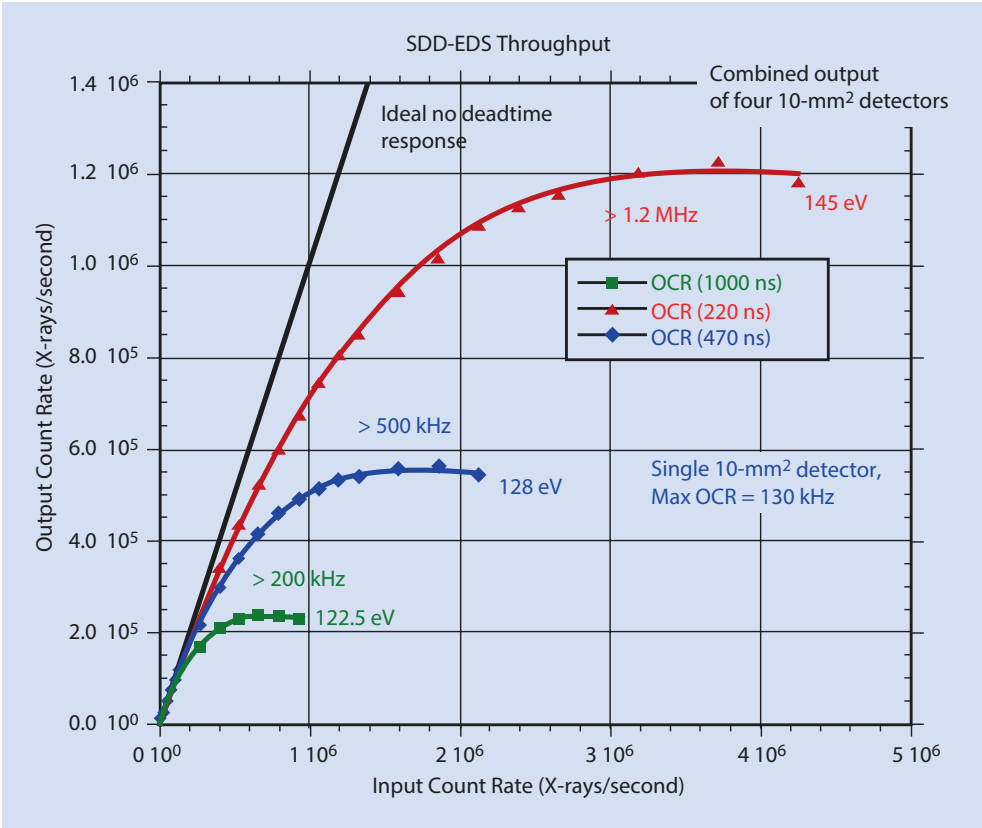

Fig. 24.22 Throughput of an SDD-EDS system consisting of four 10-mm² detectors with the outputs summed at three different operating time constants

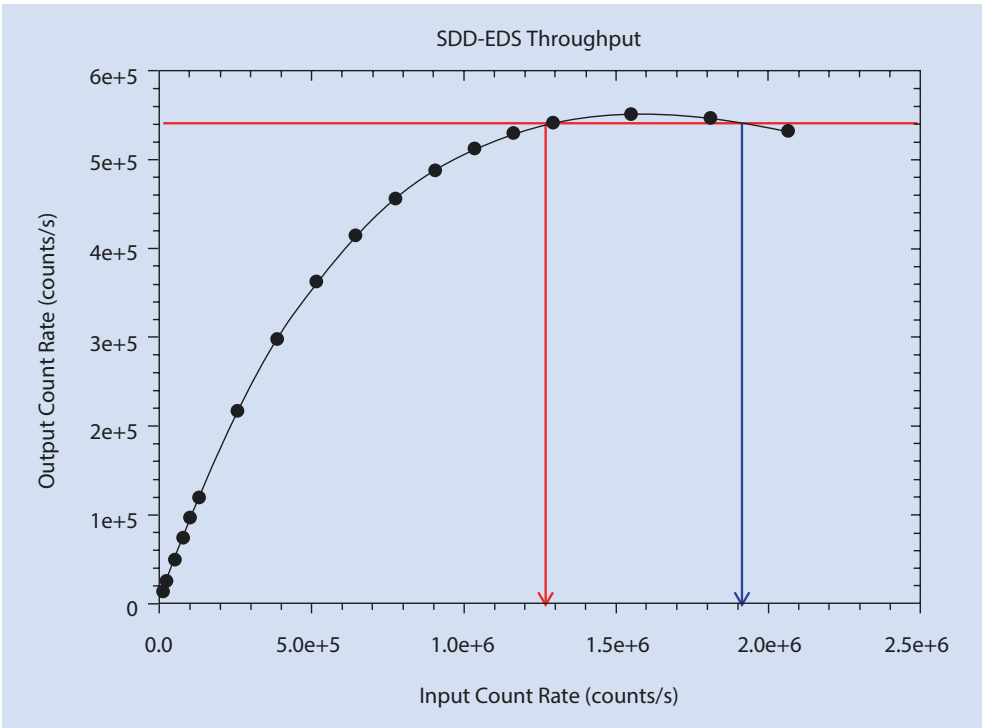

Fig. 24.23 Example of XSI mapping at such high throughput level that count rate based artifacts appear: measured OCR vs. ICR response for an SDD-EDS, showing the same OCR for two different ICR values, which could represent different concentrations of a highly excited element

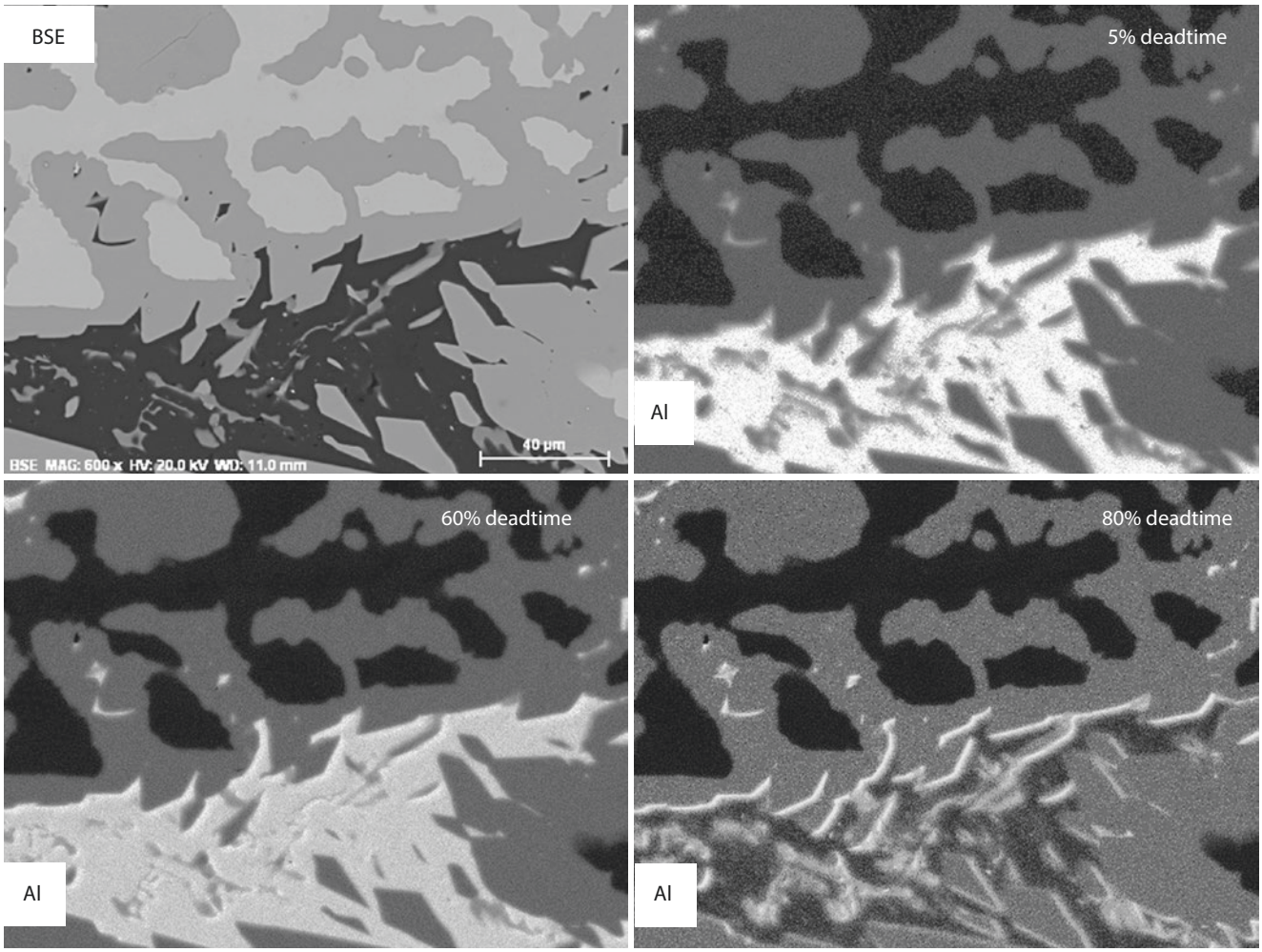

Fig. 24.24 Al map in Raney nickel recorded at 5 %, 60 %, and 80 % dead-time; note changes in the high Al region at 80 % dead-time compared to 5 % dead-time

24.4.3 Choosing the Pixel Dwell Time

Once the analyst has chosen the pixel density, the product of the number of pixels in a map and the pixel dwell time gives the total mapping time. The OCR of the EDS and the pixel dwell time determine the number of counts in the individual pixel spectra, which sets the ultimate limit on the compositional information that can be subsequently recovered from the XSI. The high throughput of SDD-EDS, especially when clusters of detectors are used, provides OCR of 10^5/s to 10^6/s, enabling various XSI imaging strategies determined by the number of counts in the individual pixel spectra.

"Flash Mapping"

By operating with a high OCR, major constituents can be mapped in less than 60 s, a mode of operation that can be termed "flash" mapping, which is useful for surveying unknowns. An example of a flash mapping survey of a leaded-brass particle is shown in Fig. 24.25, where the SEM-BSE image in Fig. 24.25a reveals a high-atomic-number inclusion. An XSI was recorded with 640 by 480 pixels with a 64-µs pixel dwell at on OCR of 750 kHz for a total mapping time of 20 s. The raw intensity maps for Cu, Zn, and Pb and their color overlay are shown in Fig. 24.25b. While very noisy on the single pixel level, these maps nevertheless reveal the localization of the lead corresponding as expected to the bright region in the SEM-BSE image. The color overlay, however, shows numerous dark areas within the particle which do not correspond to Cu, Zn, or Pb. With this short pixel dwell, the pixel level EDS spectra contain only about 50 counts total, the effect of which can be seen in the noisy derived MAXIMUM PIXEL spectrum in Fig. 24.26. (An additional derived spectrum, the RUNNING MAXIMUM PIXEL, which is averaged over three adjacent energy "cards" to reduce the effect of the low count, is also shown.) The SUM spectrum shown in Fig. 24.26, consisting of all counts recorded in 20 s, approximately 15 million, contains abundant information. In addition to the peaks for Cu, Zn,and Pb, a major peak for Ni is observed. When the raw elemental map for Ni is constructed from the XSI, the missing regions in Fig. 24.25b are filled in, as shown

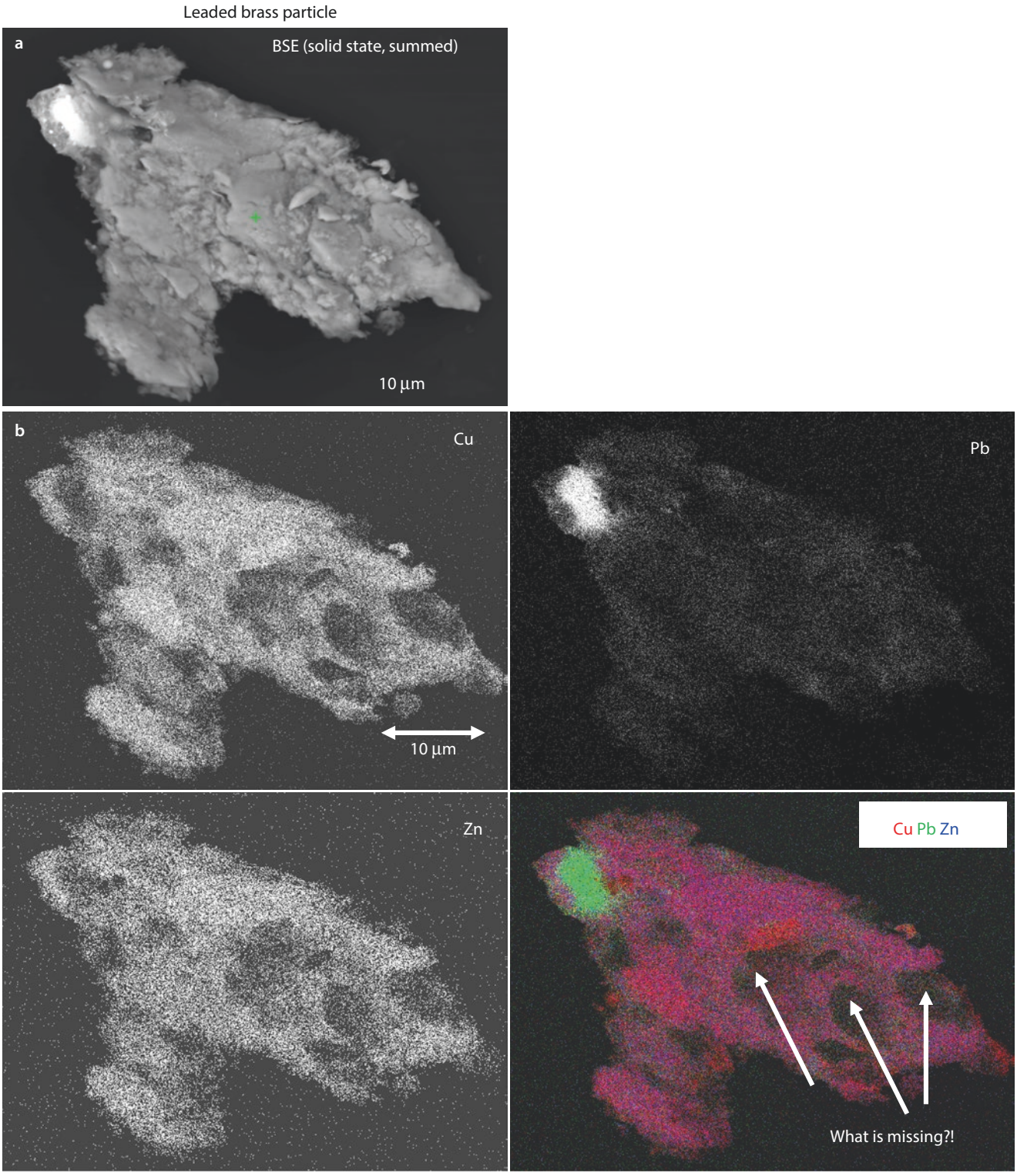

Fig. 24.25 Leaded brass particle XSI: **a** SEM-BSE image; note bright inclusion; **b** XSI recorded with 640 × 480 pixels; 64 µs/pixel = ~ 20 s total scan and total intensity images for Pb, Cu and Zn with color overlay; note apparently missing regions of particle (*dark*)

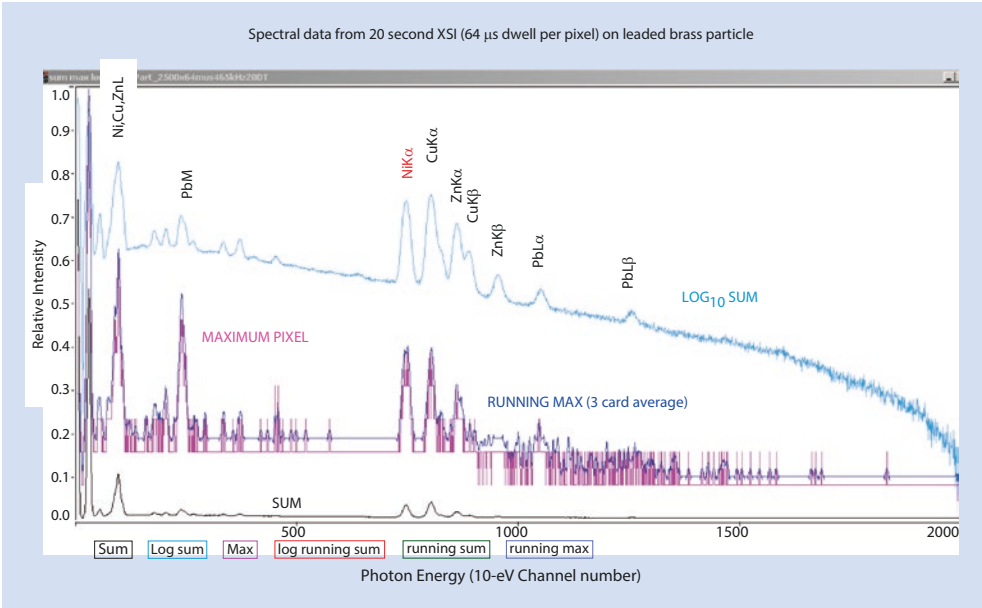

Fig. 24.26 Leaded brass particle XSI: SUM spectrum, logarithm of the SUM spectrum, MAXIMUM PIXEL spectrum, and RUNNING MAXIMUM PIXEL spectrum (averaged over three consecutive energy "cards"); note unexpected Ni peak

in Fig. 24.27, which also shows the color overlap of Cu, Zn, and Ni. This example demonstrates the value of XSI imaging to augment the information obtained from the atomic number contrast of the SEM-BSE image. In Fig. 24.27b, the SEM-BSE image easily distinguishes the Pb-rich inclusion from the brass matrix but shows no distinct contrast from the Ni-rich regions relative to the Cu-Zn brass matrix. Ni, Cu, and Zn are only separated by one unit of atomic number, so that the BSE atomic number contrast between these phases is very weak and dominated by the contrast produced by the Pb-rich region relative to the brass matrix. The SEM-BSE contrast situation is further complicated by the topographic contrast of the complex surface of the particle. Element-specific compositional imaging reveals the details of the complex microstructure of this particle.

High Count Mapping

The strategy for elemental mapping data collection depends on the nature of the problem to be solved: the most critical question is typically, "What concentration levels are of interest?" If minor and trace level constituents are not important, then short duration (60 s or less), low pixel density (256 × 256 or fewer) XSI maps with a high OCR will usually contain adequate counts, a minimum of approximately 50–500 counts per pixel spectrum, depending on the particular elements and overvoltage, to discern concentration-based contrast for major constituents, as shown in the examples in Figs. 24.25, 24.26, and 24.27. Of course, by accumulating more counts above this threshold, progressively lower concentration contrast details can be revealed for the major constituents. For problems involving minor and/or trace constituents, longer pixel dwell times are necessary to accumulate at least 500–5000 counts per pixel spectrum, and the beam current should be reduced to keep the dead-time generally below 10 % to minimize coincidence peaks. This dead-time condition can be relaxed if the coincidence peaks, which are only produced by high count rate parent peaks associated with major constituents, do not interfere with the minor/trace constituent peaks of interest.

An example of the compositional details that can be observed at the level of approximately 5000 counts per pixel spectrum is shown for a complex Zr-Ni-V alloy with minor Ti, Cr, Mn and Co in Fig. 24.28. Excellent gray-scale (after autoscaling) contrast is obtained between the phases which have relatively small changes in composition for the individual elements. Although the single pixel spectra do not have adequate counts for robust quantification, the analyst can use the images to form pixel masks that contain much higher total counts. The compositional values noted in Fig. 24.28 are based on quantifying SUM spectra taken from the two phases that are specified by the arrows in the elemental maps, and the very small statistical error reported reflects the very high count SUM spectra.

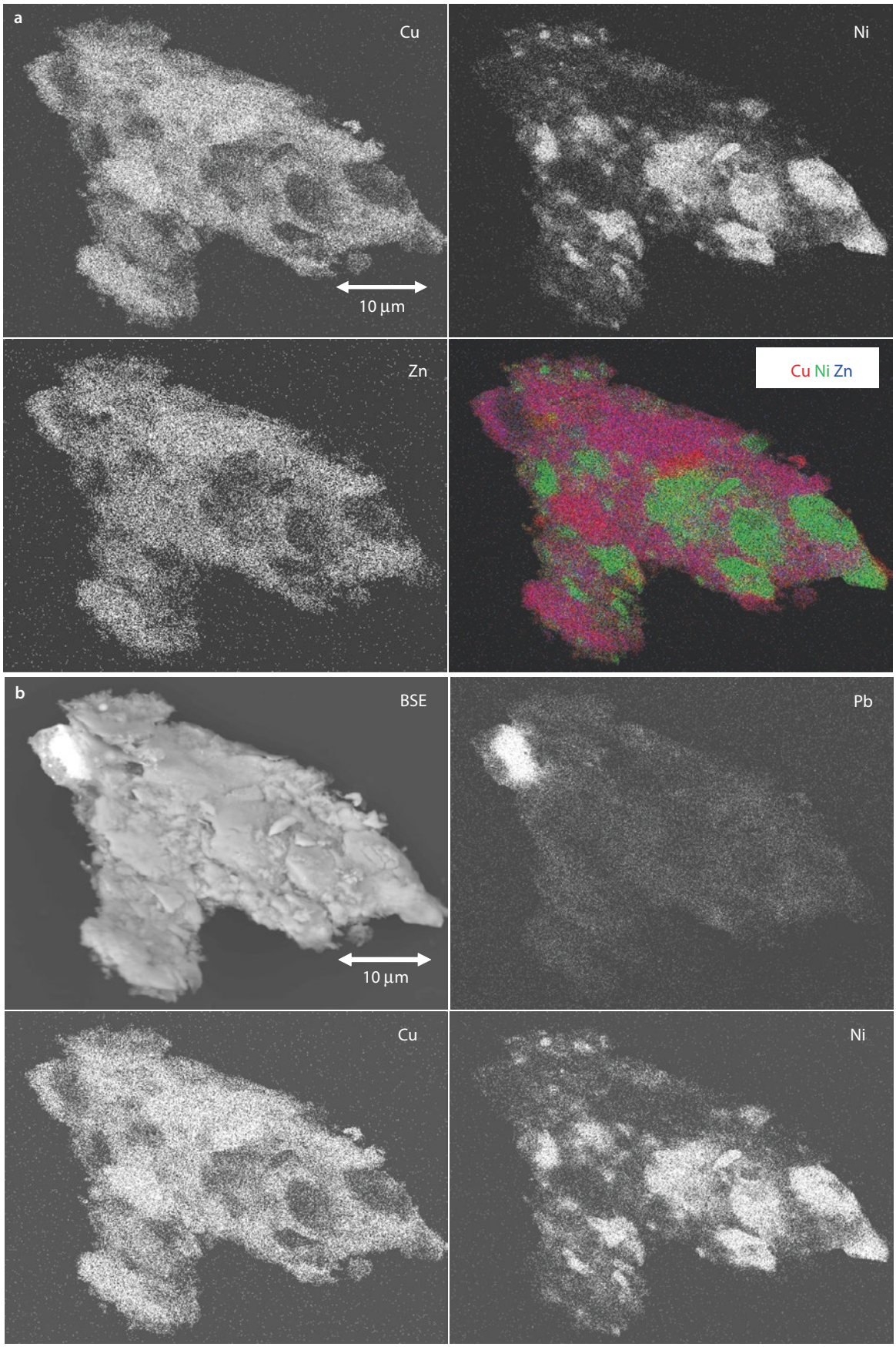

Fig. 24.27 Leaded brass particle XSI: **a** total intensity images for Cu, Zn, and Ni with color overlay showing Ni filling in empty areas seen in Fig. 24.25b; **b** direct comparison of SEM-BSE image and Cu, Ni, and Zn total intensity maps; the SEM-BSE image is insensitive to the compositional contrast between the Cu-Zn regions and the Ni-rich regions

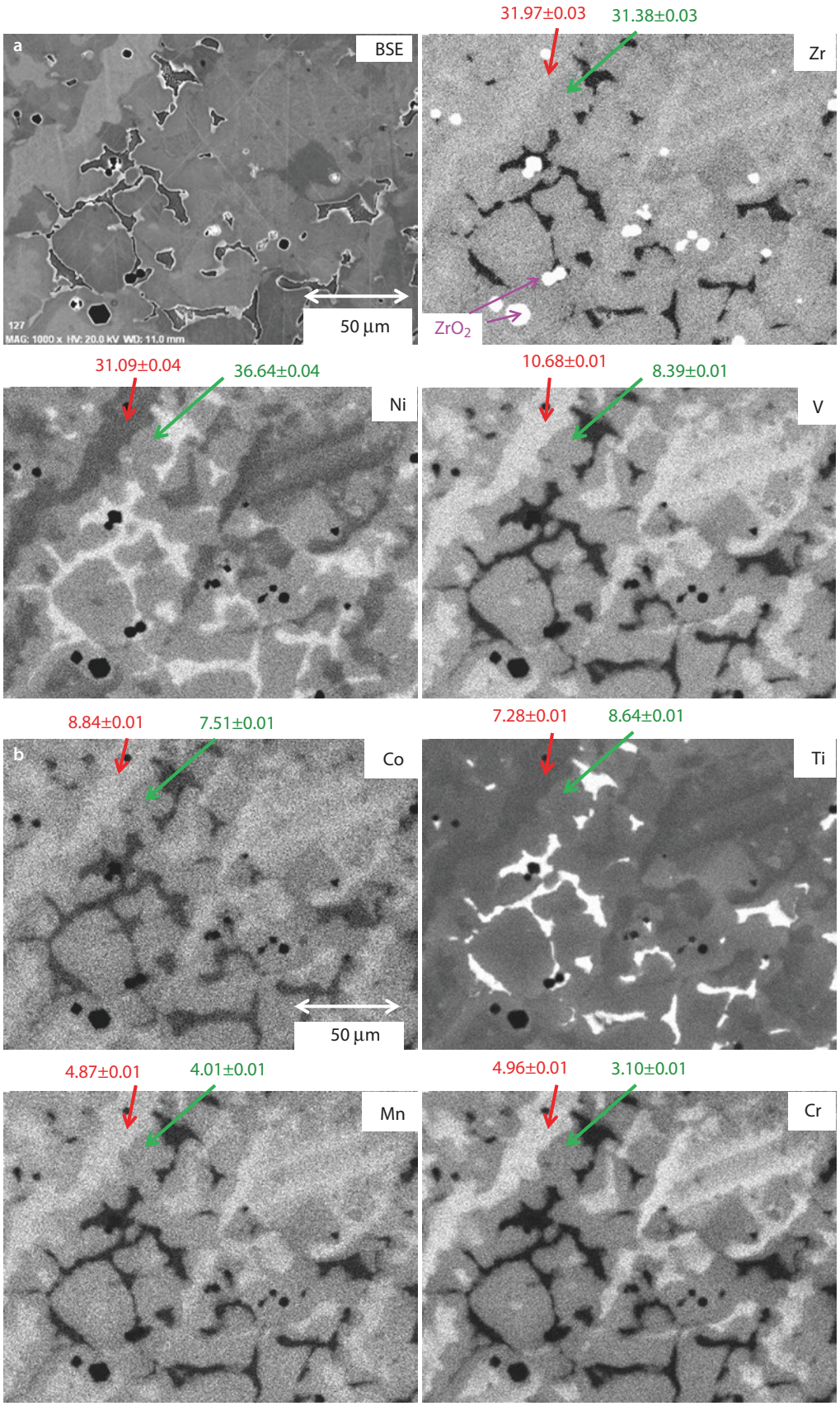

Fig. 24.28 Deep gray level mapping of Ni-Zr-V (with minor Ti, Cr, Mn, and Co) hydrogen-storage alloy (XSI conditions: 512 × 384 pixels, 8192 µs = 27 min; OCR 637 kHz = ~ 5200 counts/pixel spec): quantitative compositional maps with autoscaled gray level presentation for **a** major constituents and **b** minor constituents. Compositional values noted are derived from SUM spectra formed from pixel masks of the phases marked by *arrows*

References

Bright D (2017) NIST Lispix, a software engine for image processing, available free at: ► http://www.nist.gov/lispix/doc/contents.htm

Bright D, Newbury D (2004) Maximum pixel spectrum: a new tool for detecting and recovering rare, unanticipated features from spectrum image data cubes. J Microsc 216:186

Gorlen KE, Barden LK, Del Priore JS, Fiori CE, Gibson CC, Leapman RD (1984) Computerized analytical electron microscope for elemental mapping. Rev Sci Instrum 55:912

Kotula P, Keenan MR, Joseph R, Michael JR (2003) Automated analysis of SEM X-ray spectral images: a powerful new microanalysis tool. Microsc Microanal 9:1

Newbury D, Bright D (1999) Logarithmic 3-band color encoding: Robust method for display and comparison of compositional maps in electron probe X-ray microanalysis. Microsc Microanal 5:333

Newbury D, Ritchie N (2013) Elemental mapping of microstructures by scanning electron microscopy –energy dispersive X-ray spectrometry (SEM-EDS): extraordinary advances with the Silicon Drift Detector (SDD). J Anal At Spectrom 28:973